Evidence from polymict ureilite meteorites for a disrupted and re-accreted single ureilite parent asteroid gardened by several distinct impactors

Hilary Downes [a,b,*], David W. Mittlefehldt [c], Noriko T. Kita [d], John W. Valley [d]

[a] *School of Earth Sciences, Birkbeck University of London, Malet Street, London WC1E 7HX, UK*
[b] *Lunar and Planetary Institute, 3600 Bay Area Boulevard, Houston, TX 77058, USA*
[c] *Mail Code KR, NASA/Johnson Space Center, Houston, TX 77058, USA*
[d] *Department of Geology and Geophysics, University of Wisconsin-Madison, 1215 W. Dayton St., Madison, WI 53706, USA*

Abstract

Ureilites are ultramafic achondrites that exhibit heterogeneity in mg# and oxygen isotope ratios between different meteorites. Polymict ureilites represent near-surface material of the ureilite parent asteroid(s). Electron microprobe analyses of >500 olivine and pyroxene clasts in several polymict ureilites reveal a statistically identical range of compositions to that shown by unbrecciated ureilites, suggesting derivation from a single parent asteroid. Many ureilitic clasts have identical compositions to the anomalously high Mn/Mg olivines and pyroxenes from the Hughes 009 unbrecciated ureilite (here termed the "Hughes cluster"). Some polymict samples also contain lithic clasts derived from oxidized impactors. The presence of several common distinctive lithologies within polymict ureilites is additional evidence that ureilites were derived from a single parent asteroid.

In situ oxygen three isotope analyses were made on individual ureilite minerals and lithic clasts, using a secondary ion mass spectrometer (SIMS) with precision typically better than 0.2–0.4‰ (2SD) for $\delta^{18}O$ and $\delta^{17}O$. Oxygen isotope ratios of ureilitic clasts fall on a narrow trend along the CCAM line, covering the range for unbrecciated ureilites, and show a good anti-correlation with mineral mg#. SIMS analysis identifies one ferran lithic clast as an R-chondrite, while a second ferran clast is unlike any known meteorite. An exotic enstatite grain is derived from an enstatite chondrite or aubrite, and another pyroxene grain with $\Delta^{17}O$ of $-0.4 \pm 0.2‰$ is unrelated to any known meteorite type.

Ureilitic olivine clasts with mg#s < 85 are much more common than those with mg# > 85 which include the melt-inclusion-bearing "Hughes cluster" ureilites. Thus melt was present in regions of the parent ureilite asteroid with a bulk mg# > 85 when the asteroid was disrupted by impact, giving rise to two types of ureilites: common ferran ones that were residual after melting and less common magnesian ones that were still partially molten when disruption occurred. One or more daughter asteroids re-accreted from the remnants of the mantle of the proto-ureilite asteroid. Polymict ureilite meteorites represent regolith that subsequently formed on the surface of a daughter asteroid, including impact-derived material from at least six different meteoritic sources.
© 2008 Elsevier Ltd. All rights reserved.

1. INTRODUCTION

Ureilites are the second largest group of achondrites. They are ultramafic meteorites composed of mostly of olivine and pyroxene with lesser amounts of elemental carbon, sulfide and metal (Goodrich, 1992; Mittlefehldt et al., 1998). Their high carbon content, roughly 3 wt% on average, distinguishes ureilites from other achondrites. The carbon occurs mostly as graphite, but shock-produced diamond and lonsdaleite are present in many ureilites. We will refer to the assemblage of carbon minerals as "carbon phases". The silicate mineral compositions of ureilites

* Corresponding author.
E-mail address: h.downes@ucl.ac.uk (H. Downes).

clearly indicate the loss of a basaltic component through igneous processing, yet the suite is very heterogeneous in mg# (molar $100 * (MgO/(MgO+FeO))$). Another distinguishing characteristic of ureilites is their extremely heterogeneous oxygen isotopic compositions that are very similar to those of the carbonaceous chondrite anhydrous mineral (CCAM) line (Clayton and Mayeda,1988, 1996) which may reflect heterogeneity in their chondritic precursors. The mg# heterogeneity may have been inherited from the nebula (Clayton and Mayeda,1988, 1996) or may have resulted from combined igneous and redox processes acting on the parent asteroid (Walker and Grove, 1993; Singletary and Grove, 2003; Goodrich et al., 2007).

Despite numerous studies, the exact origin of ureilites remains unclear. It is generally accepted that typical ureilites are the basalt-depleted remains of partial melting of a chondritic precursor (Mittlefehldt et al., 1998). Some ureilites, particularly augite-bearing ureilites, may be partially of cumulate origin (Goodrich et al., 2001). The ~4.56 Ga U–Pb age (Torigoye-Kita et al., 1995) and recent studies of short-lived chronometers (Goodrich et al., 2002; Kita et al., 2003; Lee et al., 2005) indicate that the parent asteroid of the ureilites differentiated very early in the history of the Solar System. Therefore, they contain important information about processes that formed small rocky planetesimals in the early Solar System.

Because of the compositional heterogeneity, it has not yet been firmly established whether ureilites were derived from a single parent asteroid or from multiple parents (see Warren et al., 2006). Indeed, the wide variation in mineral mg#s and oxygen isotope ratios could be readily explained by an origin in multiple compositionally similar parent asteroids that had experienced a similar evolution. If all ureilites are derived from a single parent asteroid, then it cannot have achieved isotopic and chemical homogenization, i.e., it did not experience a magma-ocean stage. On the other hand, if they are derived from numerous different asteroids with different Fe/Mg ratios and oxygen isotope compositions, then the processes that formed them must have been extremely common in at least one region of the early Solar System. In either case they form a crucial test of our understanding of the formation of achondritic planetesimals from chondritic precursors. This study attempts to investigate the origin of ureilites and determine whether there are multiple parent asteroids for ureilites or just one, by examining the compositions of minerals in polymict ureilites (i.e., regolith breccias from asteroidal surfaces) and comparing them to unbrecciated (also known as "monomict") ureilites.[1]

There are currently 203 recognized ureilites (census through Meteoritical Bulletin, No. 91), which reduce to approximately 140 individual samples when pairing is taken into account. Most ureilites are unbrecciated. The cores of silicate minerals in each unbrecciated ureilite are homogeneous in cation composition. Thus, only a maximum of ~140 data points are available from these rocks to constrain the composition of the ureilite parent asteroid(s). However, there are 17 known brecciated ureilites, most being polymict, although some of these are paired. Each thin-section of a polymict ureilite may contain hundreds of clasts of ureilitic material, and multiple thin-sections greatly increase the number of clasts available for analysis. Polymict ureilites also contain lithic clasts of material indigenous to the ureilite parent asteroid but not known as discrete meteorites. Therefore the potential for studying the parent asteroid(s) of ureilites is much greater if polymict samples are analyzed.

We have undertaken a detailed study of mineral compositions in polymict ureilite meteorites that provide information about the regolith of their parent asteroid(s). We have analyzed over 500 mineral or lithic clasts from six polymict ureilites. Our goals were to evaluate whether ureilites were derived from a single parent asteroid, to gain further understanding of the evolution of the parent asteroid, and to understand ureilite petrogenesis.

2. ANALYTICAL METHODS

2.1. Electron microbeam techniques

The polymict ureilites were investigated petrographically by SEM, using back-scatter electron images. The electron microprobe analyses were done using the Cameca SX100 wavelength dispersive electron microprobe at NASA Johnson Space Center. An average was taken of three spots per grain. Analytical conditions were 20 kV, 40 nA, 1 μm beam for olivine and pyroxene. For olivine, counting times were 120 s for Ca, Cr and Mn, and 40 s for Mg, Si and Fe. For pyroxenes, counting times were 120 s for Mn, 100 s for Na, Al and Ca, 80 s for Ti, 60 s for Cr, and 20 s for Mg, Si and Fe. High and low background counts were each half the duration of the peak counts. A Mn garnet was used as the Mn standard, Cr metal for that element, and kaersutite for all other elements. Data reduction was done using the Cameca PAP data reduction routine.

Up to one hundred individual silicate mineral clasts, and a much smaller number of lithic clasts, were selected from the polished sections of each sample. A wide range of clast and grain sizes was analyzed. Other criteria for selection included a wide range of contrast in BSE images in an effort to obtain coverage of the variation in Fe contents in the clasts. Reported analyses were made only on the cores of mineral clasts, i.e., reduced rims were avoided. Representative results are given in Tables 1 (olivine) and 2 (pyroxene).

2.2. Oxygen isotope measurements

In situ oxygen three isotope analyses were carried out on three sections (Elephant Moraine (EET) 83309,51, EET

---

[1] We consider that the term "monomict" is inappropriate and redundant for unbrecciated metaigneous lithologies. Wahl (1952) originally applied the descriptor "monomict" to meteoritic breccias. The Glossary of Geology has no entry for "monomict," but defines "monomict breccia" as a textural type of rock. Further, it defines the term "monomictic" as a modifier for clastic sedimentary rocks, and lists "monomict" as a synonym. Thus, "monomict" is used in reference to clastic material. Common practice in eucrite literature is to describe them as being either "unbrecciated," "monomict," or "polymict." Here we will follow this practice and use "unbrecciated" for non-fragmental ureilites.

Table 1
Representative electron microprobe analyses of olivine grains in polymict ureilites

Sample	ts	Grain	SiO$_2$	Cr$_2$O$_3$	FeO	MnO	MgO	CaO	sum	Fe/Mn	Fe/Mg	mg#
Ureilitic olivines												
DaG 999	—	Gr45	37.8	0.58	19.9	0.415	40.5	0.321	99.54	47.4	0.276	78.4
DaG 999	—	Gr103	38.1	0.87	19.0	0.603	40.3	0.495	99.40	31.1	0.264	79.1
DaG 999	—	Gr35	38.7	0.75	18.7	0.432	40.2	0.371	99.20	42.7	0.261	79.3
DaG 999	—	Gr9	38.9	0.79	17.5	0.442	41.2	0.390	99.23	39.1	0.238	80.8
DaG 999	—	Gr88	39.4	0.74	16.3	0.447	42.2	0.376	99.49	36.0	0.216	82.2
DaG 999	—	Gr40[*]	40.0	0.59	12.8	0.592	45.2	0.288	99.48	21.3	0.158	86.3
DaG 999	—	Gr34	40.2	0.72	11.1	0.461	46.6	0.356	99.37	23.7	0.133	88.2
DaG 999	—	Gr77	40.5	0.74	9.62	0.471	47.7	0.362	99.39	20.2	0.113	89.8
DaG 999	—	Gr43	41.3	0.21	6.20	0.640	50.6	0.187	99.15	9.57	0.069	93.6
DaG 999	—	Gr26[**]	42.0	0.42	2.71	0.458	53.1	0.291	98.95	5.85	0.029	97.2
DaG1000	—	Gr23 A	38.1	0.71	22.6	0.413	37.7	0.387	99.97	54.0	0.337	74.8
DaG1000	—	Gr20	38.3	0.81	22.0	0.418	38.1	0.416	100.06	52.0	0.324	75.5
DaG1000	—	Gr16	38.6	8.60	20.8	0.447	39.3	0.286	99.97	46.0	0.297	77.1
DaG1000	—	Gr15	38.6	0.58	20.0	0.422	39.9	0.312	99.77	46.6	0.280	78.1
DaG1000	—	Gr19	41.2	0.65	8.32	0.473	49.2	0.351	100.12	17.4	0.095	91.3
DaG1023	—	Gr1	38.8	0.73	18.2	0.413	40.9	0.331	99.30	43.4	0.249	80.1
EET 83309	,51	Gr29	37.8	0.76	23.8	0.414	37.1	0.404	100.28	56.7	0.360	73.5
EET 83309	,51	Gr9	38.5	0.70	21.6	0.420	39.1	0.351	100.55	50.7	0.310	76.3
EET 83309	,50	Gr22	38.2	0.74	20.8	0.419	39.5	0.384	100.03	48.9	0.295	77.2
EET 83309	,50	Gr84	38.0	0.74	20.5	0.417	39.7	0.382	99.73	48.5	0.290	77.5
EET 83309	,51	Gr19	39.0	0.79	19.1	0.431	41.0	0.368	100.69	43.8	0.262	79.2
EET 83309	,50	Gr60	38.5	0.75	15.8	0.412	43.3	0.329	99.20	38.0	0.205	83.0
EET 83309	,51	Gr26	40.1	0.77	13.1	0.468	45.9	0.368	100.70	27.7	0.161	86.2
EET 87720	,41	Gr15	38.2	0.77	22.8	0.414	37.7	0.354	100.07	54.4	0.339	74.7
EET 87720	,41	Gr37	38.2	7.7	22.4	0.418	37.7	0.436	99.95	53.0	0.333	75.0
EET 87720	,41	Gr44	38.2	0.87	22.0	0.424	37.9	0.440	99.96	51.3	0.326	75.4
EET 87720	,41	Gr28	38.5	0.68	21.3	0.424	38.8	0.355	100.08	49.7	0.308	76.4
EET 87720	,41	Gr48	38.5	0.76	20.8	0.435	39.1	0.399	100.01	47.2	0.299	77.0
EET 87720	,41	Gr30	38.8	0.76	20.4	0.430	39.5	0.375	100.25	46.9	0.290	77.5
EET 87720	,41	Gr33	38.9	0.71	19.5	0.442	40.4	0.346	100.25	43.5	0.271	78.7
EET 87720	,41	Gr20	39.0	0.81	19.2	0.439	40.5	0.388	100.34	43.2	0.266	79.0
EET 87720	,41	Gr50	39.0	0.84	19.0	0.437	40.6	0.369	100.19	42.9	0.263	79.2
EET 87720	,41	Gr69	39.2	0.77	18.8	0.439	40.9	0.375	100.47	42.3	0.258	79.5
EET 87720	,41	Gr40	39.0	0.76	18.4	0.427	41.2	0.374	100.16	42.6	0.251	79.9
EET 87720	,41	Gr76	39.3	0.88	17.8	0.446	41.7	0.417	100.54	39.3	0.239	80.7
EET 87720	,41	Gr41	39.3	0.81	17.6	0.450	41.6	0.385	100.15	38.6	0.237	80.8
EET 87720	,41	Gr60	39.4	0.77	16.9	0.445	42.3	0.346	100.19	37.6	0.225	81.7
EET 87720	,41	Gr21	39.4	0.81	16.4	0.455	42.6	0.392	100.02	35.5	0.215	82.3
EET 87720	,41	Gr65*	40.2	0.56	12.4	0.568	46.3	0.283	12.40	21.6	0.150	87.0
EET 87720	,41	Gr38*	40.3	0.59	11.7	0.566	46.3	0.290	99.75	20.4	0.142	87.6
EET 87720	,41	Gr29	40.5	0.62	10.9	0.442	47.1	0.341	99.83	24.3	0.130	88.5
FRO 93008	—	Gr24	37.6	0.55	18.9	0.440	39.0	0.319	96.92	42.4	0.272	78.6
FRO 93008	—	Gr2[*]	39.1	0.55	12.1	0.545	44.5	0.287	97.03	21.9	0.153	86.8
Nilpena	A	Gr24	37.4	0.54	24.3	0.420	36.7	0.336	99.74	57.1	0.372	72.9
Nilpena	A	Gr36	37.9	0.49	23.2	0.412	37.5	0.284	99.76	55.7	0.348	74.2
Nilpena	A	Gr27	38.9	0.72	17.5	0.421	41.8	0.346	99.75	41.1	0.235	81.0
Nilpena	A	Gr45	39.2	0.84	16.6	0.451	42.3	0.409	99.71	36.2	0.220	82.0
Nilpena	A	Gr7	40.4	0.83	14.6	0.478	43.3	0.531	100.11	30.1	0.189	84.1
Nilpena	A	Gr28	40.7	0.64	8.14	0.463	49.3	0.346	99.58	17.4	0.093	91.5
North Haig	B	Gr34	36.7	0.35	28.5	0.539	32.1	0.313	98.46	52.1	0.497	66.8
North Haig	B	Gr37	37.7	0.75	22.2	0.409	37.3	0.426	98.84	53.7	0.335	74.9
North Haig	B	Gr18	38.2	1.07	21.0	0.424	37.6	0.504	98.75	49.0	0.314	76.1
North Haig	B	Gr49	38.1	0.86	20.3	0.418	38.8	0.432	98.84	47.9	0.294	77.3
North Haig	B	Gr61	38.4	0.72	19.6	0.445	39.5	0.403	99.02	43.5	0.279	78.2
North Haig	B	Gr11	38.6	0.75	19.3	0.418	39.5	0.335	98.90	45.6	0.274	78.5
North Haig	B	Gr4	38.9	0.78	17.0	0.421	41.3	0.403	98.89	40.0	0.232	81.2
North Haig	B	Gr48	39.3	0.67	14.5	0.471	43.5	0.347	98.85	30.5	0.187	84.2
North Haig	B	Gr19	40.1	0.74	9.87	0.498	47.3	0.310	98.79	19.6	0.117	89.5
North Haig	B	Gr35	41.0	0.70	5.54	0.503	50.5	0.357	98.51	10.9	0.062	94.2

(*continued on next page*)

Table 1 (*continued*)

Sample	ts	Grain	SiO$_2$	Cr$_2$O$_3$	FeO	MnO	MgO	CaO	sum	Fe/Mn	Fe/Mg	mg#
Non-indigenous clasts												
DaG 999	—	Gr109	35.7	0.03	33.2	0.412	29.8	0.095	99.19	79.6	0.625	61.5
DaG1000	—	Gr8	36.3	0.01	33.4	0.422	29.7	0.096	99.94	78.2	0.632	61.3
EET 83309	,51	RC	37.5	0.02	32.5	0.411	29.9	0.078	100.37	78.1	0.333	62.1
EET 87720	,41	RC	36.6	0.08	31.8	0.407	31.1	0.284	100.29	77.0	1.31	63.6
North Haig	B	Gr39	42.1	0.00	0.79	0.007	55.5	0.109	98.51	108	0.0080	99.2

∗, Hughes cluster; ∗∗, ol-aug-pig clast; RC, R-chondrite-like clasts.

87720,41 and Dar al Gani (DaG) 999) using a CAMECA IMS-1280 ion microprobe at the University of Wisconsin-Madison. The analytical conditions were modified from Kita et al. (2004), which used the older IMS-1270 in multi-collection mode. In addition to a number of improvements to the IMS-1280 hardware and software, we used

Table 2
Representative electron microprobe analyses of pyroxene clasts in polymict ureilites

Sample	ts	Grain	SiO$_2$	TiO$_2$	Al$_2$O$_3$	Cr$_2$O$_3$	FeO	MnO	MgO	CaO	Na$_2$O	sum	Fe/Mn	Fe/Mg	mg#
Ureilitic pyroxenes															
DaG 999	—	Gr8	54.3	0.05	0.66	1.14	12.8	0.409	26.0	3.89	0.07	99.34	30.8	0.275	78.4
DaG 999	—	Gr5	54.9	0.06	0.51	1.11	11.2	0.412	27.5	3.64	0.02	99.34	26.7	0.227	81.5
DaG 999	—	Gr68	55.3	0.07	0.55	1.11	9.51	0.444	28.3	3.95	0.02	99.30	21.1	0.188	84.2
DaG 999	—	Gr59a	53.1	0.30	1.56	1.35	4.21	0.407	19.6	18.4	0.23	99.20	10.2	0.120	89.3
DaG 999	—	Gr74	56.4	0.12	0.69	1.03	5.07	0.504	31.2	4.51	0.04	99.49	9.93	0.0913	91.6
DaG 999	—	Gr92	58.5	0.02	0.09	0.86	4.81	0.374	35.7	0.34	0.00	100.75	12.7	0.0755	93.0
DaG 999	—	Gr23∗∗	57.9	0.14	0.41	0.67	1.79	0.490	35.0	2.72	0.05	99.54	3.57	0.0287	97.2
DaG 999	—	Gr85	58.1	0.14	0.40	0.66	1.79	3.500	35.1	2.70	0.05	99.43	3.50	0.0286	97.2
DaG 999	—	Gr82a	55.1	0.30	0.70	0.61	1.11	0.376	22.2	18.9	0.23	99.54	2.93	0.0282	97.3
DaG 1000	—	Gr27	54.3	0.08	1.19	1.28	11.8	0.428	26.2	4.33	0.13	99.73	27.2	0.253	79.8
DaG1000	—	Gr31a	53.1	0.37	1.61	1.43	4.16	0.411	19.1	19.2	0.29	99.67	9.99	0.122	89.1
DaG 1000	—	Gr5	56.1	0.11	0.73	1.03	6.32	0.449	32.0	2.57	0.04	99.36	13.9	0.111	90.0
EET 83309	,51	Gr25	53.9	0.06	0.77	1.29	13.8	0.407	25.1	4.58	0.09	99.97	33.4	0.308	76.5
EET 83309	,50	Gr92	53.8	0.04	0.46	1.15	12.7	0.405	27.0	3.52	0.03	99.13	30.9	0.263	79.2
EET 83309	,51	Gr17	54.5	0.09	1.50	1.30	11.8	0.2	28.1	2.38	0.10	100.25	29.9	0.236	80.9
EET 83309	,51	Gr16	54.5	0.08	1.49	1.29	11.8	0.393	28.2	2.38	0.09	100.20	29.6	0.235	81.0
EET 83309	,51	Gr35	55.4	0.06	0.48	1.17	11.3	0.439	27.9	3.45	0.06	100.27	25.4	0.227	81.5
EET 83309	,51	Gr11	55.7	0.08	0.50	1.16	8.37	0.477	30.0	3.96	0.03	100.35	17.3	0.157	86.5
EET 83309	,51	Gr18a	53.2	0.24	1.97	1.28	4.32	0.424	20.2	18.4	0.15	100.12	10.1	0.120	89.3
EET 83309	,51	Gr5a	53.3	0.27	1.72	1.43	4.15	0.397	19.8	18.9	0.28	100.32	10.3	0.118	89.5
EET 83309	,50	Gr44	56.1	0.10	0.50	1.06	5.65	0.507	31.6	4.30	0.03	99.83	11.0	0.101	90.9
EET 87720	,41	Gr58	54.6	0.04	0.56	1.25	13.3	0.409	26.0	3.93	0.04	1032.00	32.0	0.287	77.7
EET 87720	,41	Gr26	54.3	0.06	0.77	1.24	12.6	0.409	25.7	4.38	0.04	99.48	30.3	0.275	78.5
EET 87720	,41	Gr1	54.2	0.05	0.80	1.28	12.1	0.410	25.3	5.12	0.04	99.29	29.1	0.269	78.8
EET 87720	,13	Gr36	53.7	0.02	0.23	1.14	13.2	0.354	30.6	0.58	0.00	99.80	37.9	0.243	80.6
EET 87720	,13	Gr08	55.3	0.07	0.67	1.26	9.54	0.449	28.9	3.24	0.05	99.45	21.0	0.185	84.4
EET 87720	,13	Gr40	56.0	0.01	0.173	1.02	9.73	0.336	31.7	0.55	0.00	99.53	28.6	0.173	85.3
EET 87720	,41	Gr14	56.8	0.09	0.70	0.84	7.61	0.389	31.7	1.91	0.05	100.05	19.3	0.135	88.1
Nilpena	A	Gr9	54.7	0.06	0.63	1.15	11.9	0.414	27.9	2.64	0.08	99.56	28.5	0.240	80.7
Nilpena	A	Gr29	54.9	0.04	0.53	1.30	10.7	0.464	27.9	3.47	0.08	99.44	22.8	0.216	82.3
Nilpena	A	Gr46	55.4	0.14	0.96	1.15	7.18	0.565	29.1	5.38	0.05	99.84	12.5	0.139	87.8
Nilpena	A	Gr19a	52.8	0.23	1.87	1.42	4.48	0.406	19.5	18.5	0.23	99.43	10.9	0.129	88.6
North Haig	—	Gr58	54.2	0.04	0.42	1.13	12.7	0.392	26.6	3.06	0.02	98.53	32.0	0.268	78.8
North Haig	—	Gr3	54.8	0.07	0.70	1.13	10.8	0.423	27.3	3.84	0.02	98.94	25.1	0.221	81.9
North Haig	—	Gr16	55.0	0.09	0.85	1.06	9.05	0.424	28.1	4.22	0.07	98.81	21.1	0.181	84.7
North Haig	—	Gr69	55.4	0.11	0.67	09.1	7.66	0.391	31.6	2.37	0.03	99.16	19.4	0.136	88.0
Non-indigenous pyroxenes															
EET 83309	,51	RC	55.1	0.05	0.16	0.07	19.5	0.388	24.5	0.923	0.02	100.71	49.5	0.446	69.1
EET 83309	,50	RC	54.4	0.05	0.18	0.08	19.3	0.395	24.7	0.938	0.03	100.18	48.3	0.439	69.5
EET 83309	,51	Gr20	57.5	0.09	0.52	0.80	4.21	0.498	34.2	2.48	0.03	100.27	8.34	0.0691	93.5
EET 83309	,50	Gr31	58.7	0.05	0.12	0.03	0.89	0.109	39.4	0.409	0.02	99.70	8.04	0.0126	98.8
EET 83309	,51	Gr1	59.6	0.00	0.11	0.01	0.36	0.005	40.0	0.180	0.01	100.21	71.0	0.0051	99.5

a, augite; ∗∗, ol-aug-pig clast in DaG 999; RC, R-chondrite-like clast.

high primary Cs^+ ion intensities of 6 nA ($\sim15\,\mu m$ spot diameter) and obtained high secondary $^{16}O^-$ ion intensities of 5×10^9 cps (Kita et al., 2007). In these conditions, all three oxygen isotopes are measured using Faraday Cup detectors with sufficient S/N ratios. Detailed analytical parameters are described in electronic annex EA-1. The instrumental mass fractionation factors of olivine and pyroxene are evaluated using terrestrial standard minerals with known $\delta^{18}O_{VSMOW}$ values. The typical external errors of repeated San Carlos olivine standard analyses on different spots of homogeneous standards were 0.3–0.4‰ (2SD) for $\delta^{18}O$, $\delta^{17}O$ and $\Delta^{17}O$ ($=\delta^{17}O - 0.52 \times \delta^{18}O$), which we consider to be the uncertainty of individual spot analyses (Table EA-1). For comparison, previous SIMS analyses typically have uncertainties (2SD) for individual spot analyses of ~1.5‰ for $\delta^{18}O$ and 1.5–5‰ for $\delta^{17}O$ (Aléon et al., 2002; Jones et al., 2004; Krot et al., 2006). Kita et al. (2004) achieved better precisions down to 0.3‰ and 1‰ for $\delta^{18}O$ and $\delta^{17}O$, respectively, which still show significantly large errors on $\delta^{17}O$ compared to the total range of variations observed among ureilites (<3‰).

3. PETROGRAPHY OF SELECTED POLYMICT UREILITES

Samples investigated in this study include two from Elephant Moraine Antarctica (EET 83309, EET 87720), two from Australia (North Haig, Nilpena) and two from Libya (DaG 999, DaG 1000). The Elephant Moraine samples were obtained as interior chips. Dar al Gani ureilites were purchased as small slices. Two sections were investigated from each of EET 87720 (sections 13, 41), EET 83309 (sections 50, 51), North Haig (A, B) and Nilpena (A, B), and one section from each of the two DaG samples. The four Elephant Moraine sections were each made from a separate chip. The North Haig sections were provided by the Western Australia Museum (sample number 12809), and C. Goodrich kindly loaned us two thin sections of Nilpena.

Goodrich et al. (2004) provided a comprehensive review of polymict ureilites, including all of the samples examined in this study. EET 83309, EET 87720 and Nilpena contain solar-wind implanted gases, indicating derivation from regolith (Rai et al., 2003). Warren and Kallemeyn (1989, 1992) reported the bulk compositions of EET 83309 and EET 87720. Guan and Crozaz (2000, 2001) reported electron microprobe and ion microprobe results for EET 87720 and EET 83309. Cohen et al. (2004) presented electron microprobe analyses of melt-derived feldspathic clasts in DaG 164, DaG 165, DaG 319, DaG 665 and EET 83309. Ikeda et al. (2000, 2003) and Ikeda and Prinz (2001) studied the compositional variation of mineral clasts in DaG 319, while Kita et al. (2004) investigated their oxygen isotope compositions. Jaques and Fitzgerald (1982) presented a petrologic description of Nilpena, including descriptions of several individual clasts.

Descriptions of clasts in numerous polymict ureilites are given in Cohen et al. (2004), Ikeda and Prinz (2001), Ikeda et al. (2000, 2003) and Jaques and Fitzgerald (1982), and the reader is referred to these sources for details of textures and mineralogies of various clast types. Here we will focus only on a broad outline of the petrography of these rocks. Fig. 1 contains large-scale views of two of our EET samples showing typical textures of polymict ureilites. The rocks are composed of numerous angular to rounded mineral and lithic clasts of diverse types, but dominated by typical ureilitic material—olivine, low-Ca pyroxene and carbon phases. Clast sizes are variable and there is no clear distinction between what might be considered small clasts and matrix. The rocks are generally matrix-poor, and within individual thin sections different areas can be clast-supported or matrix-supported breccia.

Our sections of EET 87720 contain numerous ureilitic olivine and pigeonite clasts that have been shocked to different extents, as well as rare exotic grains of albitic plagioclase, nearly pure forsterite and nearly pure enstatite. There are a number of strongly zoned ureilitic olivines with Mg-rich rims spotted with Fe-metal. Several sections of this meteorite contain large clasts (>1.5 cm) of shocked mosaicised ureilite, composed of olivine with interstitial pigeonite, set in a brecciated matrix dominated by fragments of ureilitic olivine and pyroxene. EET 87720,41 also contains a large (0.5 cm) clast of a coarse-grained lithology composed of ferran olivine with subordinate sodic plagioclase, rare pyroxene and pyrrhotite (irregular, light gray clast in upper center of upper panel, Fig. 1).

Our sections of EET 83309 are mostly formed of angular clasts of olivine, pigeonite and rare augite, all within the ranges of compositions known from unbrecciated ureilites, together with single large mineral clasts of enstatite (Gr1, lower panel, Fig. 1), plagioclase (including some of pure anorthite composition) and a single grain of chromite. Single grains of ureilitic olivine are up to 0.1 cm in diameter, but most are much smaller. Both sections contain rock clasts at least 0.2 cm across, containing ferran olivine with subordinate plagioclase, pyroxene, chromite and pyrrhotite. One of these is shown in Fig. 1, lower panel. The different cosmic-ray exposure (CRE) ages of EET 83309 and EET 87520 (Rai et al., 2003) demonstrate that they are not paired.

North Haig was found in western Australia (Berkley et al., 1980; Prinz et al., 1983). One of the two sections (section A) is composed of a single lithic clast. Section B is a typical polymict breccia, containing a wide variety of olivine and pyroxene clasts up to 0.2 cm in diameter, together with some plagioclase clasts and carbon phases. Nilpena is from South Australia (Jaques and Fitzgerald, 1982). Both of our sections consist of a coarse-grained polymict breccia containing angular and rounded clasts of olivine, pigeonite and augite, together with abundant carbon phases, rare plagioclase and a few melt clasts. The possibility of North Haig being paired with Nilpena was discussed by Prinz et al. (1986) but discounted (Prinz et al., 1987).

Russell et al. (2003) have previously described DaG 999 and DaG 1000. The section of DaG 999 shows a coarse-grained graphite-bearing polymict ureilite that contains a large (0.5 cm diameter) clast of an augite-bearing ureilite lithology. A second large clast (1 cm diameter) is composed of olivine-pigeonite ureilite. DaG 999 also contains an exotic clast of a ferran olivine lithology, and grains of pure anorthitic feldspar. The section of DaG 1000 contains

abundant angular and rounded clasts of olivine, pigeonite and augite up to 0.5 cm in diameter, displaying various levels of shock, two non-indigenous clasts of a ferroan olivine lithology similar to those described in EET 87720, abundant carbon phases and several grains of plagioclase.

4. RESULTS

4.1. Olivine compositions

Olivine core compositions of 34 unbrecciated ureilites were previously analyzed at JSC (Hudon and Mittlefehldt,

data in EA-2) using the analytical protocols used in this study. Almost all olivines from these samples fall on the previously established ureilite Fe/Mn vs. Fe/Mg trend of Goodrich et al. (2004) (see Fig. 1 of EA-2). Olivine core mg#s range from 76 (Graves Nunataks (GRA) 98032) to 95 (Allan Hills (ALH) 82130), thus covering the entire range of known ureilite compositions. Olivines from unbrecciated ureilites display narrow ranges of minor element contents (0.38–0.55 wt% MnO, 0.26–0.42 wt% CaO and 0.4–0.9 wt% Cr_2O_3) in agreement with previous studies (see Mittlefehldt et al., 1998). As already noted by Goodrich et al. (2004), several poikilitic-textured orthopy-
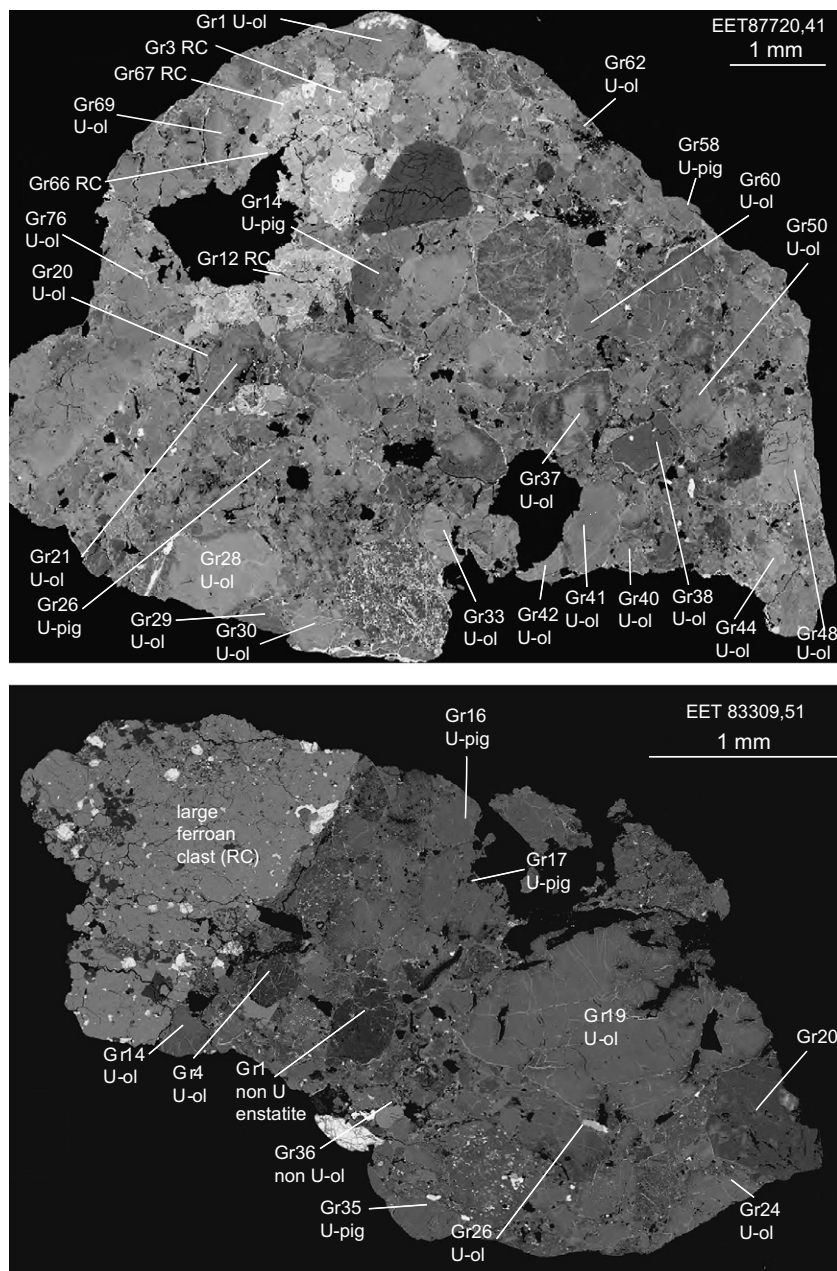
Fig. 1. BSE images of representative sections of two polymict ureilites (EET 87720, EET 83309) examined in this study. Section EET 87720,41 is approximately 1 cm across. Section EET 83309,51 is approximately 0.5 cm in longest dimension. Clasts analyzed by SIMS for oxygen isotopes are indicated by grain number. "U-ol", ureilitic olivine; "U-pig", ureilitic pigeonite. "RC", R-chondrite-like ferroan lithic clast.

roxene-bearing EET samples (EET 87511, EET 87523, EET 87717, EET 96322, EET 96328 and EET 96262) are paired, all having mg#s of 84.9. Olivines from several augite-bearing Antarctic ureilites (EET 96314, EET 96331 and EET 96293) have identical olivine compositions (mg#s = 86.8) and textural features and must therefore be paired. However, they plot below the ureilite trend, and thus have slightly higher Mn/Mg values, and are very similar in composition to those of olivines from the unusual augite-bearing ureilite Hughes 009 (Goodrich et al., 2001). Olivines from unbrecciated ureilites and olivine clasts in polymict ureilites with compositions similar to those in Hughes 009 will be referred to subsequently as the "Hughes cluster" (Fig. 2).

More than 330 olivine clasts have been analyzed from the six polymict samples. A selection of the data is presented in Table 1. The vast majority of olivine clasts in the polymict ureilites display very similar range of CaO and Cr_2O_3 contents to those in olivine in unbrecciated ureilites (0.2–0.5 wt% CaO; 0.4–0.9 wt% Cr_2O_3). Olivines with compositions greatly outside these values are considered to be non-indigenous. Fig. 2 shows the complete data set for olivines, including non-indigenous clasts, from all six samples plotted on the conventional Fe/Mg vs. Fe/Mn diagram (Mittlefehldt, 1986). All of the polymict ureilites contain a wide range of olivine compositions that fall on the ureilite trend, covering the entire compositional range of unbrecciated ureilites. In addition DaG 999 and EET

87720 contain a few ureilitic olivine clasts whose compositions are identical to those found in Hughes 009, thus forming part of the "Hughes cluster". Olivines from the large olivine-augite-pigeonite clast in DaG 999 (Gr26 in Table 1) are very highly magnesian (mg# 97) but have 0.32 wt% CaO and 0.49 wt% Cr_2O_3, well within the normal range of olivines from unbrecciated ureilites. The discovery of this clast extends the range of compositions of ureilites to mg# 97, beyond that of unbrecciated ureilites (for which the most Mg-rich is ALH 82106 with mg# 94).

Olivines from the ferroan olivine clasts in several polymict samples have a narrow range of compositions (mg# 59–65; four of the non-indigenous grains listed in Table 1) and clearly plot beyond the range of the ureilite trend (Fig. 2). Their NiO contents are ca. 0.5 wt%, in contrast to ureilitic olivines which have <0.01 wt% NiO (Goodrich et al., 1987), and their Cr contents (<0.08 wt% Cr_2O_3) are much lower than in ureilitic olivines. A few less abundant olivine clasts have much lower MnO contents, low Mn/Mg ratios and, in some cases, low CaO and Cr_2O_3 contents. They plot above the ureilite trend (Fig. 2). According to Jaques and Fitzgerald (1982) and Ikeda et al. (2000), they are probably derived from chondritic impactors on the surface of the ureilite parent asteroid. Two other olivine clasts (North Haig B-Gr34 and DaG 999-Gr103) have higher Mn/Mg ratios than normal ureilite olivines and lie off the array (Fig. 2). They have CaO and Cr_2O_3 concentrations that are close to those of normal ureilitic olivines and resemble olivines in
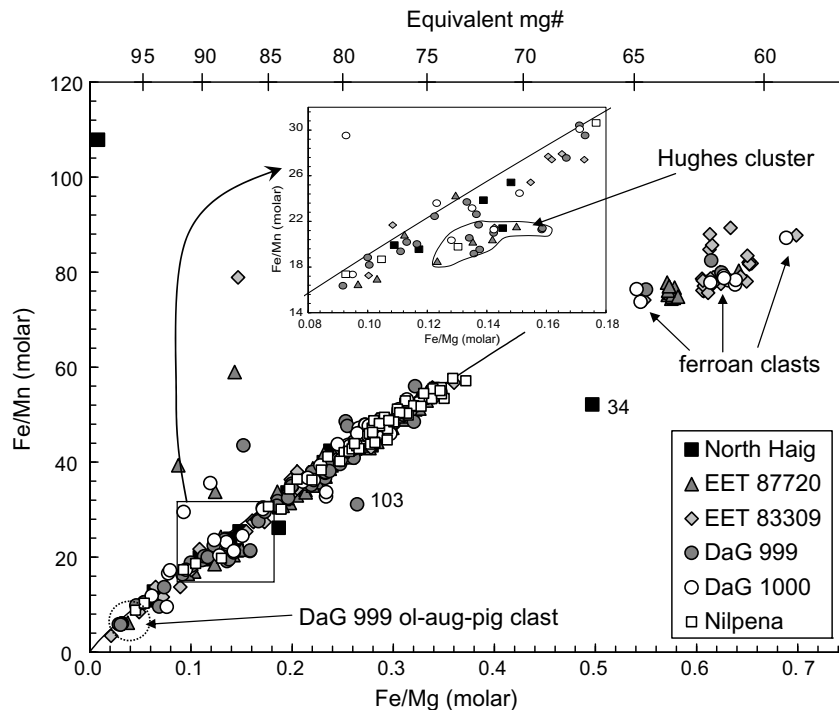

Fig. 2. Fe/Mn vs. Fe/Mg molar compositions of all olivines from clasts and single mineral grains analyzed from polymict ureilites in this study compared to the ureilite trend of Goodrich et al. (2004) (solid line). Grains labeled 103 and 34 are DaG 999 Gr103 and North Haig B Gr34 (Table 1). These have ureilitic contents of CaO and Cr_2O_3 but higher Mn/Mg ratios and may be derived from ureilitic melt clasts. The inset shows details of the Hughes cluster olivines, which are displaced below the ureilite Fe/Mn–Fe/Mg trend compared to other ureilites. Olivines from a very magnesian olivine-augite-pigeonite clast from DaG 999 are located in the dashed circle, indicated.

igneous melt-clasts from polymict ureilites (Ikeda et al., 2000; Cohen et al., 2004). Thus they may be derived from disruption of such ureilitic melt clasts, but this cannot be confirmed without further oxygen isotope analyses.

Data for olivine clasts from each polymict sample show as wide a spread of Fe/Mn vs. Fe/Mg compositions as all unbrecciated ureilites. Most of the data are in the Fe-rich range (Fe/Mg = 0.20–0.36; mg# = 83–74), similar to the distribution of unbrecciated ureilite suite (Mittlefehldt et al., 1998). Ureilitic olivine compositions in all polymict ureilites start abruptly at Fe/Mg values of 0.36 (mg# 74). There appears to be a compositional gap between Fe/Mg = 0.16 and 0.19 (mg# 84 and mg# 86) in EET 87720, North Haig and DaG 1000. The distributions of olivine compositions from all six polymict samples are generally similar, but not identical. Since they have different CRE ages, the polymict ureilites were excavated during several different impact events and the compositional distributions may reflect different relative contributions of "source regions" locally exposed on the parent asteroid(s).

Fig. 3 presents a histogram of mg# in all ureilitic olivine clasts from the six polymict samples. Care has been taken to remove examples of repeat analyses of the same clast (e.g., the large mosaicised clast in EET 87720,13) and exotic clasts such as those derived from chondrites. The distribution of compositions is broadly similar to that reported for unbrecciated ureilites by Goodrich et al. (2004), with a major peak at mg# 78–79. However, a minor peak at mg# 86–87 is present in the polymict olivine data that does not coincide with the peaks seen in data from individual unbrecciated ureilites. The new data fill in the apparent gaps at mg# 83 and mg# 89 seen in unbrecciated samples (Mittlefehldt et al., 2005) and thus predict that unbrecciated ureilites of these compositions must exist but have not yet been found. The histogram derived from the compositions of polymict clasts clearly confirms the observation of Ikeda et al. (2000) that there is a much higher proportion of ure-

ilitic olivines with mg# < 85 than those with mg# > 85. Note that the two data sets are not rigorously comparable, however. The data for the unbrecciated ureilites are a random sampling of material being delivered to Earth from the ureilite parent asteroid, while some degree of human selection has been used to acquire the polymict data set. Whether ureilite meteorites of a composition similar to the large augite-bearing ureilitic clast in DaG 999 (mg# = 97) will be found in the future remains an open question. However, from the data shown in Fig. 3, we suggest that most future ureilite finds will be part of the main group with olivine mg#s < 85.

4.2. Pyroxene compositions

Pyroxenes from the 34 unbrecciated ureilites analyzed by Hudon and Mittlefehldt (data in EA-2) are mainly pigeonites with subordinate orthopyroxenes and rare augite. They plot on a similar Fe/Mn–Fe/Mg trend to that seen in ureilitic olivines. More than 180 pyroxene clasts from the polymict ureilites have been analyzed (representative analyses, Table 2), including some augite clasts. Fig. 4 shows that the wide range of Fe/Mn and Fe/Mg in polymict ureilitic pyroxenes is similar to the range in the whole suite of unbrecciated ureilites. In addition to the pyroxenes that fall on the trend shown by unbrecciated ureilites, polymict ureilites contain pyroxene clasts with low Mn/Mg ratios that plot well above the ureilite trend and are probably derived from non-ureilitic impactors. Several pyroxenes mainly from DaG 1000 and Nilpena have slightly high Mn/Mg ratios, similar to that of pyroxenes in Hughes 009 (Fig. 4). Furthermore, numerous pyroxene compositions form a sub-horizontal trend towards higher Fe/Mg ratios, with little change in Fe/Mn ratio. This trend is identical to that shown by pyroxenes in igneous clasts of the "albitic lithology" analyzed by Cohen et al. (2004) from various polymict ureilites (melt clast field in Fig. 4). Pyroxenes that show this trend are probably fragments of similar
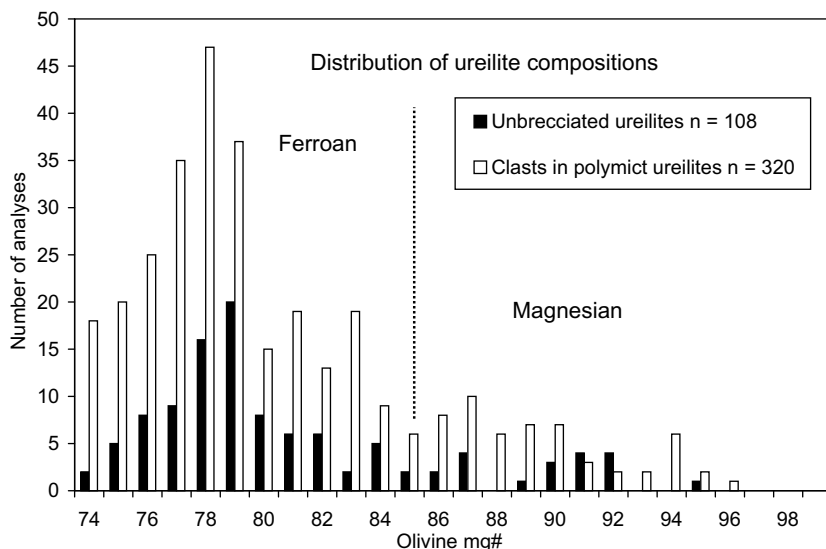

Fig. 3. Histogram of mg# in olivine in ureilite clasts and single mineral grains from polymict ureilites in this study, compared with the distribution of mg# in olivine in unbrecciated ("monomict") ureilites given by Goodrich et al. (2004).
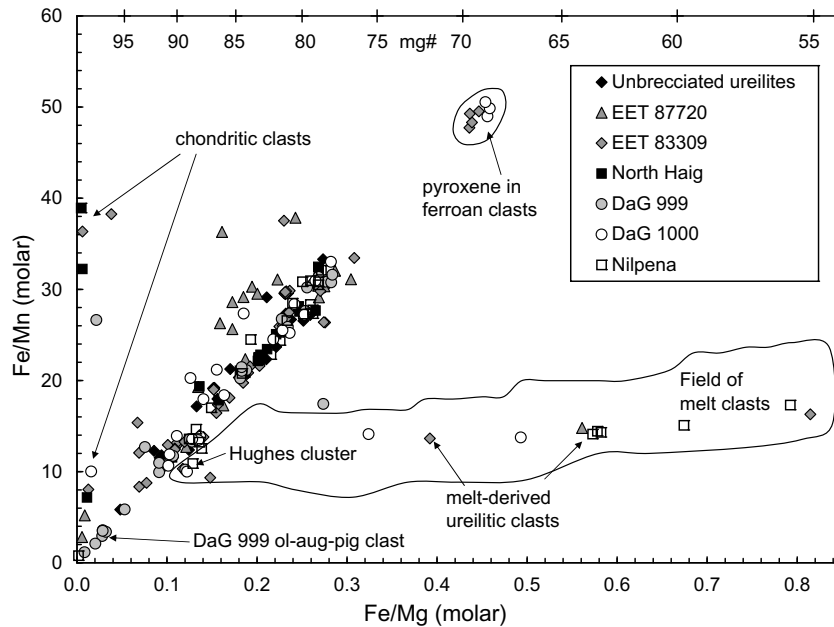
Fig. 4. Fe/Mn vs. Fe/Mg molar compositions of pyroxenes from unbrecciated and polymict ureilites analyzed in this study and by Hudon and Mittlefehldt (data in EA-2). The field labeled ''melt clasts'' is that of pyroxene analyses by Cohen et al. (2004) for grains in melt clasts found within polymict ureilites. Several pyroxenes within the low Fe/Mg end of the ''melt clasts'' field are Hughes cluster grains, as indicated.

ureilitic igneous clasts. This igneous trend appears to intersect the main ureilite trend near to the composition of the ''Hughes cluster'' samples, some of which contain melt inclusions.

Mosaicised clasts mainly in EET 87720 contain pyroxenes with slightly lower Mn/Mg ratios than normal ureilitic pigeonites, i.e., they plot above the main ureilite trend in Fig. 4. Pigeonites and augites from the olivine-augite-pigeonite clast containing mg# 97 olivine in DaG 999 are highly magnesian (mg# = 97). Chondritic enstatite pyroxenes with very high mg#s and very low Ca contents (<0.4 wt% CaO) occur in most of the polymict samples.

Fig. 5 shows the Ca contents and mg#s of pyroxenes from unbrecciated and polymict ureilites. In an EMP study of unbrecciated Antarctic ureilites, augite has been found as very rare small rounded inclusions in olivine in ureilite EET 87517 and as an abundant interstitial phase in the paired stones EET 96293, EET 96314 and EET 96331. Rare single mineral clasts of augite in DaG 1000, DaG 999, Nilpena, North Haig and EET 83309 cluster around the composition of augites from the ''Hughes cluster'' (Hughes 009, EET 96293, Frontier Mountains (FRO) 93008, etc.). The highly magnesian augites from the large olivine-augite-pigeonite ureilite clast in DaG 999 resemble those from the most magnesian ureilite ALH 82106. The remaining augite clasts from EET 83309 and EET 87720 have mg#s < 75. These clasts, as well as the pigeonites with mg#s < 75 found mainly in Nilpena, are probably derived from the breakup of igneous-textured clasts similar to those described by Cohen et al. (2004) and hence may represent some of the missing basalt melts of the ureilite parent asteroid. Exotic clasts of chondritic diopside were also found in North Haig and Nilpena. Orthopyroxenes from the ferroan

clasts tend to have mg#s in the range 68–70 and low CaO contents (<0.05 apfu).

4.3. Oxygen isotope compositions

The in situ oxygen isotope data from 15 μm spots on ureilitic and non-ureilitic clasts are shown in Table 3. Six ureilitic clasts, 1 ferroan clast and 1 enstatite single grain were analyzed in section EET 83309,51 and 20 ureilitic clasts and one large ferroan clast in section EET 87720,41. The highly Mg-rich ureilite clast in DaG 999 (Gr26) was also analyzed. Some of the larger clasts were measured in more than one spot (e.g., DaG 999 Gr26 was analyzed 5 times), though none of these clasts showed internal heterogeneity in oxygen isotope ratios. The oxygen isotope compositions of individual clasts are shown in Fig. 6, and $\Delta^{17}O$ values are plotted against mg# in Fig. 7. Fig. 6 shows that, although the ion microprobe data have larger analytical errors than the earlier bulk analyses of much larger samples, the in situ data obtained in this study plot tightly on the CCAM line defined by Clayton and Mayeda (1996). Furthermore, most ureilitic clasts plot within the range of data for unbrecciated ureilites (Clayton and Mayeda, 1996). However, one magnesian pigeonite single grain clast (EET 83309,51, Gr20) significantly deviates in oxygen isotopic compositions from the ureilitic region. The $\Delta^{17}O$ of this clast ($-0.4‰$) is at the high end of the ureilite range, but it has a high mg# (93.5) and deviates from the ureilitic trend in Fig. 7. It may be an exotic clast that was not previously distinguished by its chemical composition. Olivine in the most magnesian ureilitic clast (DaG 999 Gr26, mg# 97) yielded the most negative $\Delta^{17}O$ value ($-2.09 \pm 0.16‰$) and extends the mg# $-\Delta^{17}O$ correlation beyond that seen in unbrecciated ureilites (Fig. 7).
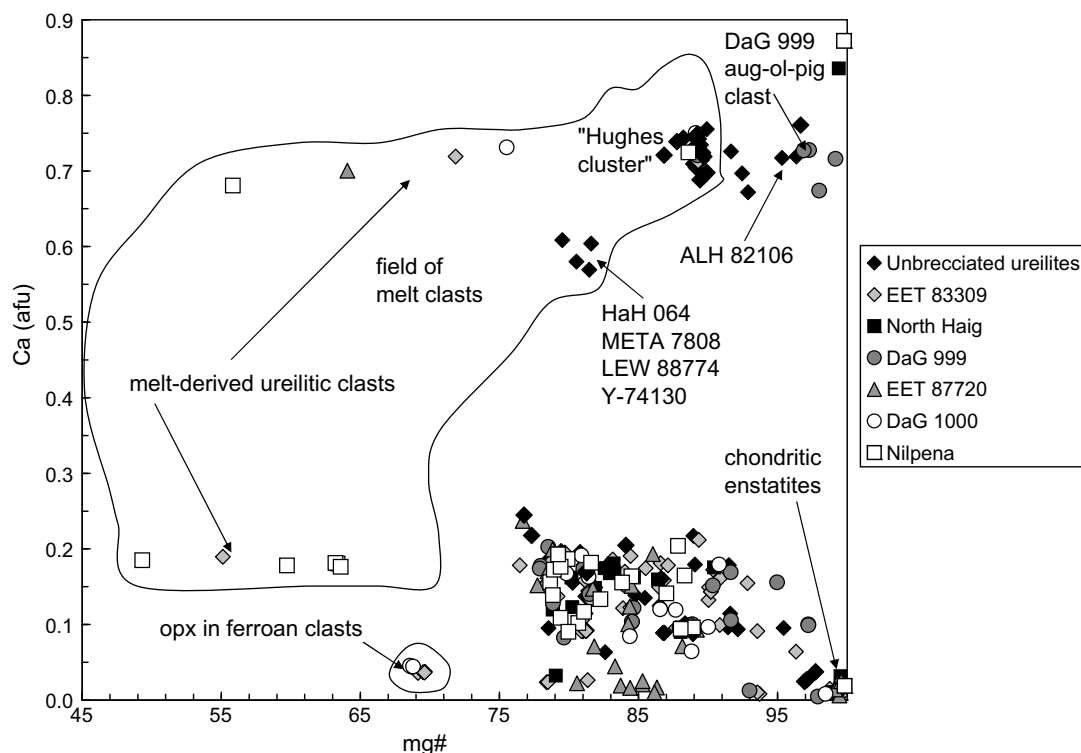
Fig. 5. Ca (afu) vs. mg# for pyroxenes from unbrecciated and polymict ureilites analyzed in this study and by Hudon and Mittlefehldt (data in EA-2). The field labeled ''melt clasts'' is that of pyroxene analyses by Cohen et al. (2004) for grains in melt clasts found within polymict ureilites. Several grains within the upper right portion of the ''melt clasts'' field are Hughes cluster grains, as indicated.

One of the ureilitic olivine clasts analyzed in this study, EET 87720,41 Gr38, is characterized as being part of the ''Hughes cluster'' from its Mn content (Table 1 and Fig. 2). Data from this clast plot on the CCAM line in Fig. 6, though the $\Delta^{17}O$ value of -1.2% is slightly off the mg# $- \Delta^{17}O$ trend compared to other magnesian samples in Fig. 7. The oxygen isotopic compositions of this clast are in good agreement with those of Hughes 009 (Clayton and Mayeda, 1996) within analytical errors. Ikeda and Prinz (2001) studied carbon-free clasts in polymict ureilite DaG 319 that resemble Hughes 009, their ''type II ureilitic clasts''. The oxygen isotope ratios of these type II clasts are also consistent with that of Hughes 009 (Kita et al., 2004).

Two ferroan clasts plot in completely different locations on the 3-isotope diagram (Fig. 6); one from EET 83309,51 plots in the region close to R-chondrites, but the other clast from EET 87720,41 plots very near to the Terrestrial Fractionation (TF) line and close to the brachinite region. The single nearly pure enstatite clast (EET 83309,51 Gr1) also plots on the TF line, consistent with derivation from an enstatite chondrite or aubrite.

5. DISCUSSION

Our petrographic observations, and electron microprobe and high precision SIMS oxygen isotope data on mineral and lithic clasts from polymict ureilites, coupled with literature data, allow us to examine several issues regarding the origin of ureilites. Here we will primarily address (i)

whether there are distinct groupings of ureilites, (ii) whether the ureilite suite was derived from more than one parent asteroid, (iii) the types of impactors that gardened ureilites to produce the polymict breccias, and (iv) the nature of the ureilite parent asteroid.

5.1. Ferroan clasts and exotic mineral grains

We have found large (0.2–0.5 cm) exotic ferroan clasts in 4 of the 6 polymict ureilites analyzed (DaG 999, DaG 1000, EET 83309 and EET 87720). Similar clasts have been reported from polymict ureilite DaG 319 by Ikeda et al. (2000, 2003), who referred to them as ''equilibrated chondrite clasts'' and noted their similarity to R-chondrites. Goodrich et al. (2004) briefly mention an equilibrated chondrite clast as being similar to R group chondrites. Cohen et al. (2004) described a ''feldspathic olivine augite'' clast C24 with an olivine composition of mg# 63 from polymict ureilite DaG 164. This clast is probably an exotic ferroan clast like those described here. Single grains of mg# 60 olivine have also been reported in FRO 93008 (Fioretti and Goodrich, 2001), FRO 90168 and FRO 90228 (Smith, 2002), most probably derived from fragmentation of ferroan clasts.

The olivine compositions, the presence of chromite and pyrrhotite, and the absence of metal in these clasts, suggest a similarity to R chondrites. However, the two ferroan clasts analyzed by SIMS have different oxygen isotope ratios (Table 3 and Fig. 6). The ferroan clast

Table 3
Ion microprobe oxygen isotope analyses of individual clasts[a]

Sample	ts	Grain	n[*]	mg#	Phase	$\delta^{18}O$ ‰	2SE	$\delta^{17}O$ ‰	2SE	$\Delta^{17}O$ ‰	2SE
Ureilitic clasts											
EET83309	,51	Gr16	1	81.0	$Wo_{4.7}En_{77.2}$	8.36	0.32	3.69	0.27	−0.66	0.29
EET83309	,51	Gr17	1	80.8	$Wo_{4.7}En_{77.1}$	7.79	0.40	3.67	0.32	−0.38	0.24
EET83309	,51	Gr19	4	79.3	$Fo_{79.3}$	7.94	0.17	3.15	0.14	−0.98	0.14
EET83309	,51	Gr26	1	86.2	$Fo_{86.2}$	6.17	0.32	1.47	0.27	−1.74	0.29
EET83309	,51	Gr35	1	81.5	$Wo_{6.7}En_{76.0}$	7.73	0.40	2.91	0.32	−1.11	0.24
EET83309	,51	Gr20[c]	2	93.5	$Wo_{4.7}En_{89.2}$	5.53	0.28	2.46	0.22	−0.42	0.17
EET87720	,41	Gr1	2	78.8	$Wo_{10.3}En_{70.7}$	8.24	0.18	3.37	0.27	−0.91	0.26
EET87720	,41	Gr14	1	88.1	$Wo_{3.7}En_{84.9}$	6.21	0.45	1.52	0.37	−1.71	0.29
EET87720	,41	Gr20	1	79.0	$Fo_{79.0}$	7.68	0.26	2.72	0.38	−1.27	0.37
EET87720	,41	Gr21	2	82.3	$Fo_{82.3}$	6.95	0.22	2.14	0.31	−1.48	0.25
EET87720	,41	Gr26	1	78.5	$Wo_{8.8}En_{71.6}$	8.53	0.26	3.67	0.38	−0.76	0.37
EET87720	,41	Gr28	1	76.4	$Fo_{76.4}$	8.39	0.32	3.62	0.44	−0.74	0.36
EET87720	,41	Gr29	1	88.5	$Fo_{88.5}$	5.55	0.45	0.88	0.37	−2.01	0.29
EET87720	,41	Gr30	1	77.5	$Fo_{77.5}$	8.27	0.26	3.31	0.38	−0.99	0.37
EET87720	,41	Gr33	2	78.7	$Fo_{78.7}$	7.97	0.26	2.91	0.28	−1.23	0.23
EET87720	,41	Gr37	2	75.0	$Fo_{75.0}$	8.41	0.32	4.12	0.26	−0.25	0.21
EET87720	,41	Gr38[b]	1	87.6	$Fo_{87.6}$	7.46	0.26	2.70	0.38	−1.18	0.37
EET87720	,41	Gr40	1	79.9	$Fo_{79.9}$	7.74	0.32	2.71	0.44	−1.31	0.36
EET87720	,41	Gr41	1	80.8	$Fo_{80.8}$	7.14	0.45	2.56	0.37	−1.16	0.29
EET87720	,41	Gr44	1	75.4	$Fo_{75.4}$	8.49	0.26	3.80	0.38	−0.62	0.37
EET87720	,41	Gr48	1	77.0	$Fo_{77.0}$	8.28	0.32	3.15	0.44	−1.15	0.36
EET87720	,41	Gr50	1	79.2	$Fo_{79.2}$	7.98	0.45	2.94	0.37	−1.21	0.29
EET87720	,41	Gr58	1	77.7	$Wo_{7.8}En_{71.7}$	8.69	0.45	4.28	0.37	−0.24	0.29
EET87720	,41	Gr60	1	81.7	$Fo_{81.7}$	7.35	0.26	2.51	0.38	−1.31	0.37
EET87720	,41	Gr69	1	79.5	$Fo_{79.5}$	7.69	0.45	2.98	0.37	−1.02	0.29
EET87720	,41	Gr76	1	80.7	$Fo_{80.7}$	7.48	0.32	2.57	0.44	−1.32	0.36
DaG999	—	Gr26	5	97.0	$Fo_{97.0}$	5.82	0.20	0.94	0.24	−2.09	0.16
Non-indigenous clasts											
EET83309	,51	RC	3	62.1	$Fo_{62.1}$	4.14	0.20	5.50	0.16	3.35	0.16
EET87720	,41	RC	4	63.5	$Fo_{63.5}$	3.28	0.16	1.78	0.20	0.10	0.17
EET83309	,51	Gr1	1	99.5	$Wo_{0.3}En_{99.2}$	5.64	0.40	2.88	0.32	−0.05	0.24

[a] Data are corrected for the instrumental mass fractionation by using olivine and pyroxene standards. The quoted errors are 2 standard deviations (2SD, 95% confident level) of the repeated analyses of 8-bracketed standard analyses for clasts analyzed only once. For clasts that were analyzed several times, the weighted averages and errors were obtained from the individual spot analyses shown in Table A2. RC, R-chondrite-like clasts.

[b] ¶"Hughes cluster" type according to Mn contents.

[c] EET83309,51 Gr20 has ureilitic elemental composition but non-ureilitic oxygen isotope composition.

[*] Numbers of repeated spot analyses in the same clasts.

from EET 83309,51 (RC in Table 3 and 83-RC in Fig. 6) has oxygen isotope ratios that plot within the field for R chondrites, so we conclude that this clast is indeed a fragment of an R chondrite. This is the first definitive evidence for R chondrite material in polymict ureilites. In contrast, the ferroan clast from EET 87720,41 (RC in Table 3 and 87-RC in Fig. 6) has oxygen isotopic compositions that plot within uncertainty of the terrestrial fractionation line (Fig. 6), well outside the field for R chondrites. Ikeda et al. (2003) determined the oxygen isotopic composition of one ferroan clast (equilibrated chondrite clast β 22B) that is within the rather large error limits identical to the clast from EET 87720,41. This indicates that there are two distinct populations of ferroan clasts that must have been derived from different parent bodies. Lithic clast EET 87720, 41 RC is unlike any known meteorite (although it is similar to clast DaG 319 β 22B), but must represent a parent asteroid with a

similar oxidation state to that of the R chondrite parent asteroid. The oxygen isotopic composition of the EET 87720, 41 RC ferroan clast is similar to those of brachinites (Clayton and Mayeda, 1996) which are oxidized achondrites (e.g., Mittlefehldt et al., 2003). However, brachinites are not quite as oxidized as the ferroan clasts, as they have olivine mg#s in the range 64–71 (Mittlefehldt et al., 2003). Furthermore, brachinites contain calcic pyroxenes that are not present in the ferroan clast in EET 87720,41. Thus, the EET 87720, 41 RC ferroan lithic clast appears to be quite distinct from brachinites.

Among the pyroxenes in EET 83309,51, two grains (Gr1 and Gr20 in Table 3, 83-Gr1 and 83-Gr20 in Figs. 6 and 7) have anomalous oxygen isotope compositions. Grain Gr1 plots on the terrestrial fractionation line within the field of EH and EL chondrites and aubrites (Clayton et al., 1984; Clayton and Mayeda, 1996). This grain is nearly pure enstatite ($Wo_{0.3}En_{99.2}Fs_{0.5}$) with very
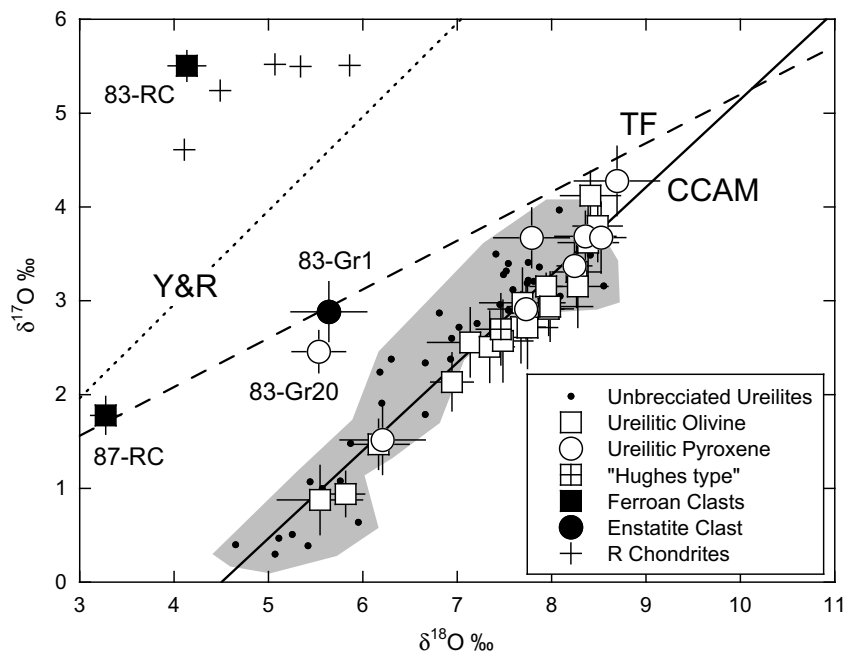
Fig. 6. Oxygen three isotope compositions of clasts in polymict ureilites EET 83309 and EET 87720. Ureilitic clasts are shown as open symbols (olivine—square, pyroxene—circle) and EET 87720, 41 Gr38, which belongs to the "Hughes cluster" is marked as a crossed square. Non-ureilitic clasts are shown as filled symbols (ferroan clasts—square and enstatite—circle). "87-RC" and "83-RC" indicate the oxidized clasts from EET 87720 and EET 83309, respectively (Table 3). "83-Gr20" indicates the analysis of grain 20 from EET 83309. Three lines labeled as "TF", "CCAM" and "Y&R" are Terrestrial mass fractionation line ($\delta^{17}O = 0.52 \times \delta^{18}O$), carbonaceous chondrite anhydrous mineral line (Clayton and Mayeda, 1996) and Young and Russell line (Young and Russell, 1998). Small dots and shadowed areas are from bulk analyses of unbrecciated ureilites (Clayton and Mayeda, 1996) and crosses are bulk R-chondrites (Weisberg et al., 1991; Bischoff et al., 1994; Shulze et al., 1994). Error bars are 2SD.
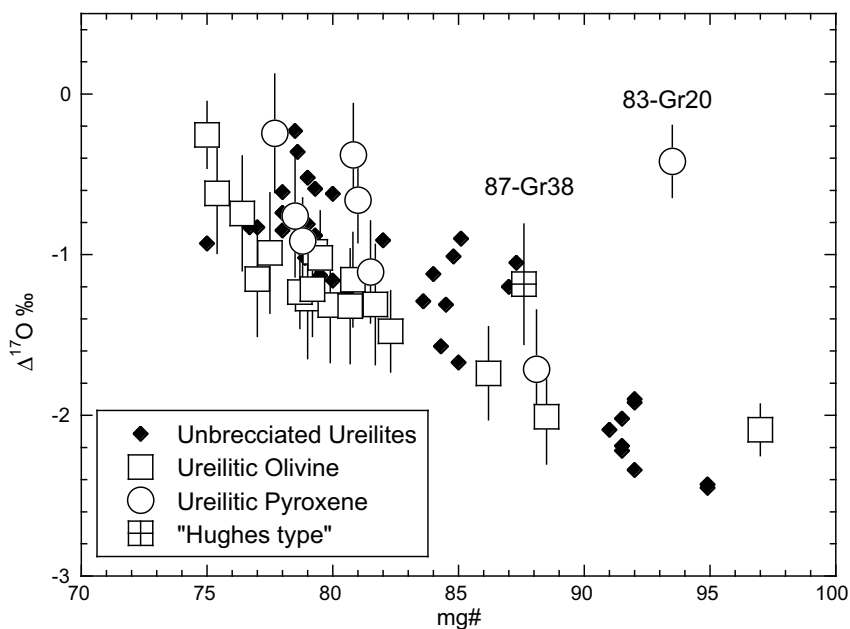
Fig. 7. Relationship between mg# and $\Delta^{17}O$ among ureilitic clasts. Symbols for polymict ureilite data are the same as in Fig. 6. The unbrecciated ureilite data (Clayton and Mayeda, 1996) are shown as small filled diamonds. Note that EET 83309, 51 Gr20 deviates significantly from the ureilite trend as in Fig. 6. 87-Gr38 is the Hughes cluster olivine EET 87720, 41 Gr38.

low minor element contents (Al_2O_3 0.11 wt%; TiO_2, Cr_2O_3, MnO and Na_2O all <0.01 wt%), similar to those of orthopyroxenes in EH and EL chondrites and aubrites (Brearley and Jones, 1998; Mittlefehldt et al., 1998).

While Gr1 plausibly was derived from an enstatite chondrite or achondrite impactor, we cannot be more specific than that. We found other pyroxenes with high mg# ($\sim$98–100) and minor element contents similar to those of Gr1 in DaG 999, EET 83309, EET 87720, Nilpena and North Haig; all of these clasts may be debris from an enstatite chondrite or achondrite parent asteroid.

Pyroxene grain EET 83309,51 Gr20 has minor element contents similar to those of ureilitic pyroxenes and plots on the ureilite Fe/Mn–Fe/Mg trend (Fig. 4), but because of its anomalous oxygen isotope composition (Fig. 6), it is not likely to be ureilitic in origin. Its oxygen isotope composition is similar to those of winonaites and silicates in IAB irons (Clayton and Mayeda, 1996) and its mg# (93.5) is within the range of those in these meteorites (Mittlefehldt et al., 1998). However, the CaO content of this grain is 2.5–3.4 times those of winonaite-IAB orthopyroxenes, and Al_2O_3 and Cr_2O_3 are higher and TiO_2 lower compared to orthopyroxenes in these other meteorites (Benedix et al., 2005). Therefore, grain EET 83309,51 Gr20 is not likely to be from the winonaite/IAB silicate parent asteroid. We conclude that this grain most likely represents debris from an unknown parent object.

A group of unusual olivines, characterized by low MnO contents and mg#s in the range of 87–92, plots well above the ureilite trend (Fig. 2). Although they have Cr_2O_3 and CaO contents within the range of normal ureilitic olivines, we concur with Ikeda et al. (2000) and Jaques and Fitzgerald (1982) that these are most likely chondritic debris. We also found one nearly pure forsterite grain (North Haig B, Gr39) which has an mg# 99.2, Cr_2O_3 and MnO contents at the detection limits, low CaO content, and Fe/Mn = 108. This grain is clearly foreign debris on the ureilite parent asteroid and was possibly derived from an enstatite chondrite- or achondrite-like parent.

It is clear from the data described above that the analyzed exotic mineral and lithic clasts are derived from a variety of parent bodies and must have been present as meteoritic debris on the surface of the ureilite asteroid. Thus, as previously discussed by Kita et al. (2004), polymict ureilites contain minor amounts of materials that originated from different parent bodies, some of which may not completely match the currently sampled meteorite groups. We estimate that at least six impactor bodies are represented; R chondrite, low-Mn ordinary chondrite (Ikeda et al., 2003), enstatite clan, carbonaceous clan ("dark clasts" as described by Prinz et al., 1987; Clayton and Mayeda, 1988; Brearley and Prinz, 1992), the parent body of grain EET 83309,51 Gr20, and angrites (Prinz et al., 1986; Kita et al., 2004). This is different from observations of the HED regolith, where only two impactors seem to dominate (CM and CR chondrites, see Zolensky et al., 1996) and these likely represent a fairly narrow range of the solar system judging by their similar chemistries and oxygen isotope compositions. The foreign debris in ureilites not only was derived from a greater number of sources, but the range in oxygen isotope composition and mineral chemistry implies that they sample a much wider range of the solar system, including both reduced and oxidized regions.

5.2. Ureilite groupings?

In this section, we will examine the results of our study to see if ureilites form a single compositional suite or if they fall naturally into separate groups according to their mineralogy and/or mineral compositions. Several previous studies have divided ureilites into different groups. For example, Goodrich et al. (2004, 2007) separated olivine-pigeonite ureilites from olivine-orthopyroxene ureilites, and considered the augite-bearing lithologies to be a separate type. However, this approach cannot be applied to single mineral clasts in polymict ureilites, as it depends on information about the mineral assemblage. Berkley et al. (1980) proposed a classification of ureilites into three groups using Fe/Mg values in olivine: Group 1 has low mg# (average $\sim$79), Group 2 has intermediate values (average $\sim$84) and Group 3 has high mg# ($\sim$91). Only eleven unbrecciated ureilites were well described at that time. Clayton and Mayeda (1988) showed that the different Berkley mg# groups also had distinctly different oxygen isotopic compositions. Franchi et al. (1997) also suggested that there were distinct groups of ureilites based on oxygen isotope compositions. This approach would be applicable to clasts in polymict breccias, but was established at a time when far fewer ureilites were known and the classification lacks an underlying rationale. Following Berkley et al. (1980), Mittlefehldt et al. (2005) divided ureilites into three groups using observed minima in the distribution of olivine compositions in unbrecciated ureilites at mg# 83 and mg# 90 in order to test for correlations with bulk chemical properties. Mittlefehldt et al. (2005) concluded that bulk compositional trends suggest that Berkley groups 2 and 3 could represent a single group distinct from Berkley group 1.

From a study of clasts in polymict ureilite DaG 319, Ikeda et al. (2000) separated Type I ureilites (olivine-pigeonite lithologies with core olivine mg#s < 84, reduction rims on olivines, and the presence of carbon phases) from Type II (olivine-orthopyroxene-augite assemblages, with mg#s > 85, lacking carbon and with little or no reduction around olivines). We have also observed that ureilite olivines with mg#s < 85 are far more common than those with mg#s > 85 (Fig. 3), so a separation into two groups appears to be well founded. The difference between the two groups of ureilitic olivines can be seen more clearly in the relation between their FeO and MnO contents in Fig. 8, in which two distinct trends can be seen. As discussed by Karner et al. (2003), olivines that have crystallized from basaltic melts show positive correlations in Fig. 8. However, on the FeO–MnO diagram, most olivine clasts from polymict ureilites form an overall negative trend, similar to that displayed by olivines from the majority of unbrecciated ureilites. All of these olivines have mg#s < 85 and most have Mn contents <0.5 wt% (only three olivine clasts have higher Mn contents). In contrast, data for olivines with mg# > 85 are much more scattered, both for unbrecciated ureilites and clasts in polymict ureilites. This scattered group includes the highly magnesian olivine-augite-pigeonite clast in DaG 999, the unusual paired augite-bearing ureilites ALH 83120, ALH 81206 and ALH 84136, and the low-Mn ureilites Yamato (Y-) 74659 and EET 87517 (the latter
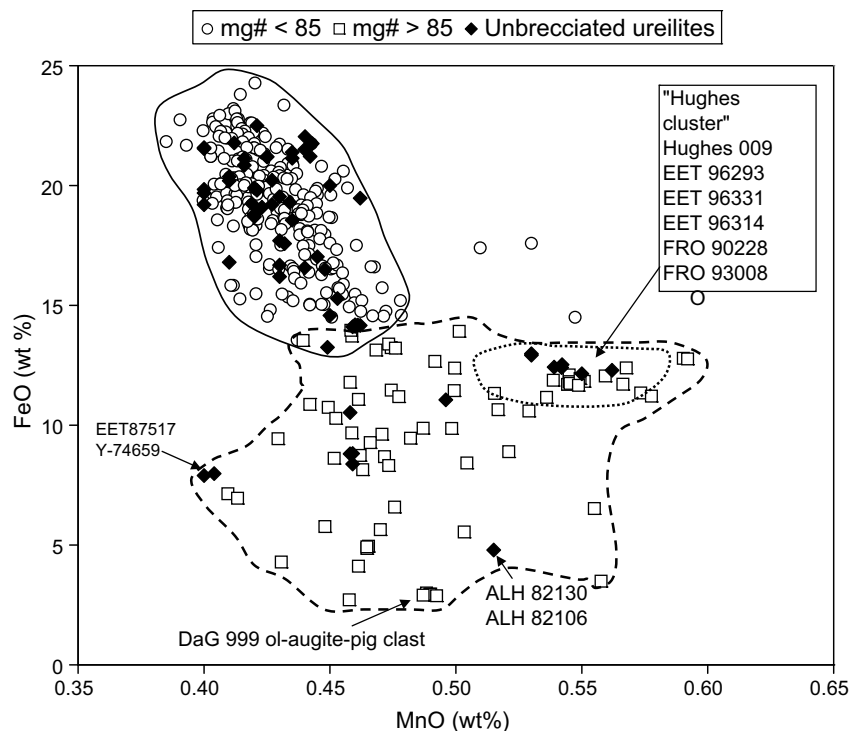
Fig. 8. FeO vs. MnO (wt%) contents in ureilitic olivines from unbrecciated and polymict ureilites analyzed here and by Hudon and Mittlefehldt (data in EA-2) with literature data from Goodrich et al. (1987), Treiman and Berkley (1994), Takeda (1987), Torigoye-Kita et al. (1995), Smith (2002) and Singletary and Grove (2003).

also augite-bearing). High-Mn contents of olivines also appear in the "Hughes cluster", i.e., augite-bearing ureilites Hughes 009, EET 96314, EET 96331, EET 96293, and FRO 90054, FRO 90228 and one lithology in FRO 93008, together with olivine clasts from polymict ureilites that have very similar compositions. Fig. 8 also shows that the compositional range of olivine clasts in polymict ureilites is very similar to that of unbrecciated ureilites, even including low-Fe, low-Mn olivines similar to those of EET 87517 and Y-74659 and high-Mn Hughes-like varieties.

A further distinction that can be made among unbrecciated ureilites is a textural one. Most ureilites display a granoblastic texture with triple junctions between silicate crystals and metal along grain boundaries (Berkley, 1986). However, a few ureilites (e.g., Pecora Escarpment (PCA) 82506, Reckling Peak (RKPA) 80239 and Lewis Cliff (LEW) 85440) have poikilitic textures. Poikilitic low-Ca pyroxene is also closely associated with the "bimodal" texture reported in Meteorite Hills (META) 78008, Y-74130, EET 87511 and ALH 82130 (Mittlefehldt et al., 1998). Other poikilitic or bimodal ureilites that have not been well studied yet include DaG 879 and FRO 01088. The paired Antarctic ureilites EET 87511, EET 87523, EET 87717, EET 96322, EET 96328 and EET 96262 all show poikilitic textures, as does the augite-bearing low-carbon lithology of FRO 93008 (Smith, 2002). Ureilites that show this texture probably formed by a different petrogenetic process than those that show more typical ureilitic textures. The texture generally is strongly reminiscent of that of some terrestrial

igneous cumulates and Goodrich (1986) has interpreted poikilitic textures in orthopyroxene- and augite-bearing ureilites as being due to cumulus processes.

Like terrestrial ultramafic rocks, ureilites could be classified on the basis of modal mineral proportions. Although modal proportions of phases in ureilites are hard to estimate because of the coarse grain-size and the small areas of typical petrographic thin-sections, nevertheless it is clear that most ureilites contain > 40% olivine (see Mittlefehldt et al., 1998) and are therefore peridotites. Only a few ureilites contain >60% pyroxene (e.g., LEW 88774, Hammadah al Hamra (HaH) 064, Y-74130, Hughes 009, MET 01085 and FRO 90054) and hence are pyroxenites. In the Earth's mantle, the distinction between pyroxenite and peridotite is fundamental; peridotites are broadly speaking restites after partial melting, whereas pyroxenites generally form by magmatic processes (e.g., crystal accumulation, melt impregnation) (Downes, 1997).

5.3. Augite-bearing ureilites and the "Hughes cluster"

We will now consider the significance of augite in ureilites and the nature of the "Hughes cluster". Takeda et al. (1989) first drew attention to the unusual nature of augite-bearing ureilites. According to Mittlefehldt et al. (1998) and Goodrich et al. (2004), there are eight augite-bearing ureilites: Hughes 009, LEW 85440 (paired with LEW 88012, LEW 88201 and LEW 88281), and ALH 82106 (paired with ALH 82130 and ALH 84136), EET 87511 (paired with EET 87523 and EET 87717), HaH

064, META78008, Y-74130 and LEW 88774. During this study, we found that Antarctic ureilites EET 87517, EET 96293, EET 96314 and EET 96331 also contain augite. Augite-bearing lithologies from the probable polymict ureilites FRO 90054, FRO 90228 and FRO 93008 can be added to this list (Smith, 2002). One large clast in DaG 999 also represents a highly magnesian (mg# = 97) augite-bearing ureilitic lithology. Fig. 5 demonstrates that augites from unbrecciated ureilites show a wide range of mg#s, from the highly magnesian ones in ALH 82106/ALH 82130 (mg# = 95), which closely resemble the augite-bearing clast in DaG 999, through the "Hughes cluster" compositions, to a group of ureilites with more iron-rich augites (HaH 064, META78008, LEW 88774 and Y-74130) with mg#s of 76. As discussed above, three of these samples are pyroxenites rather than peridotites. Their augites have distinctly lower Ca contents than those of the more Mg-rich varieties (Fig. 5) and, curiously, do not appear to have given rise to clasts in polymict breccias. Goodrich (1986) suggested that the augite in Y-74130 was cumulus in origin. Augite has also been found in interstitial material, interpreted as melt veins, in ureilites Y-74123 and Y-790981 (Ogata et al., 1991).

The augite-bearing Hughes 009 contains melt inclusions hosted by olivine crystals and lacks carbon phases (Goodrich et al., 2001). FRO 90054, FRO 90228 and the olivine-augite-orthopyroxene lithology in FRO 93008 also all contain little carbonaceous material (Smith, 2002) and melt inclusions have been reported from FRO 90054 (Fioretti and Goodrich, 2000; Goodrich, 2001). The high Mn/Mg ratios of olivines in all these augite-bearing ureilites resemble those of olivine in igneous-textured augite-olivine clasts in polymict ureilites reported by Cohen et al. (2004). Ureilitic pyroxene clasts in polymict ureilites form an igneous fractionation trend away from the "Hughes cluster", identical to the trend observed by Cohen et al. (2004) in pyroxenes from melt clasts (Fig. 4). This trend of increasing Fe/Mg with nearly constant Fe/Mn is an igneous fractionation trend, exhibiting no evidence for FeO reduction (see Mittlefehldt, 1986). Thus, it is most likely that the augite-bearing "Hughes cluster" was formed by melt-related processes on the ureilite parent asteroid as advocated by Goodrich et al. (2001) for Hughes 009. The presence of augite crystals at triple junctions in the paired ureilites EET 96293, EET 96314 and EET 96331 suggests that melt impregnation occurred in these samples, i.e., they were derived by interaction of an augite-bearing melt and restitic mantle minerals. The textures are identical to that in Hughes 009 itself (Goodrich et al., 2001). Furthermore, Hughes 009, type II clasts (Ikeda and Prinz, 2001; Kita et al., 2004) and clast EET 87720,41 Gr38 (this study) all show identical oxygen isotope ratios within analytical uncertainty. This suggests that a large volume of melt with homogeneous oxygen isotopic ratios was formed within the ureilite parent asteroid, and some of this melt reacted with restitic mantle material to form the "Hughes cluster".

The highly reduced magnesian metal-bearing rims on most ureilitic olivine grains indicate a period of extreme reduction, most probably due to reaction between hot olivine and graphite during rapid decompression. This observation points to the asteroid-scale disruption of the parent body or bodies (Takeda, 1987). The evidence that this disruption affected all ureilites suggests that there was only a single parent asteroid. The presence of melt inclusions in Hughes cluster ureilites, and the similarity of the lowest Fe/Mg pyroxene compositions of ureilite melt clasts to those of the Hughes cluster (Fig. 4), suggests that melt was still present within the parent body of these meteorites when disruption occurred to the parent body.

5.4. One or more ureilite parent asteroids?

We will now discuss the evidence for there being only one single parent body for ureilites. Scott et al. (1993) and Warren and Kallemeyn (1992) observed that existing data did not require a single ureilite parent asteroid. Goodrich et al. (2004) qualitatively showed that collectively, the polymict ureilites show a similar olivine core mg# distribution as unbrecciated ureilites, and that they share a common P–T history. She argued that this favored formation on a single ureilite parent asteroid. Nevertheless, Warren et al. (2006) concluded that the database was insufficient to determine whether a single parent asteroid produced the ureilite suite. We have analyzed more than 300 ureilitic olivine clasts in polymict ureilites, so that the statistics of our study (as shown below) are much more robust than those of previous studies and allow for quantitative assessment of the issue.

The range of the main components within each individual polymict ureilite is very similar to that of the unbrecciated ureilites (Fig. 3). We have tested this by performing a non-parametric Mann–Whitney two-tailed test on olivine mg#s. We randomly sampled 100 olivine gains from our data on DaG 999, DaG 1000, EET 83309, EET 87720, Nilpena and North Haig, and 100 randomly sampled unbrecciated ureilites using our data plus literature data. We eliminated suspected exogenous olivine grains, discussed above, from the database on polymict ureilites before sampling. The null hypothesis—that the sample populations are not different—is accepted at the 99% confidence level. Thus, statistically, the olivine populations in polymict ureilites and the unbrecciated ureilites are not significantly different in mg#. This similarity is extremely unlikely to be the case if unbrecciated ureilites were derived from a series of different parent asteroids. Oxygen isotope data for clasts in the polymict samples plot exactly within the range of unbrecciated ureilites (Fig. 6). They also show the same anti-correlation between mg# and $\Delta^{17}O$ (Fig. 7) that is observed among unbrecciated ureilites. These results are consistent with the chemistry of these clasts being complete matches to the range seen among unbrecciated ureilites and support the premise that there is only one ureilite asteroid. Thus we conclude that there is only one single parent asteroid for all ureilites.

On the other hand, individual polymict ureilites can have somewhat different distributions of olivine compositions. We performed the same statistical test on endogenous olivine grains comparing the population from each meteorite to each of the others. The results are shown in Table 4. The population of olivines in Nilpena is dis-

tinct from that of each of the other polymict ureilites at the 99% confidence level. However, most polymict ureilites are not distinguishable from each other based on their olivine populations. Table 4 shows that, whereas DaG 999 is statistically indistinguishable from North Haig, and North Haig is statistically identical to EET 83309, the statistics show that DaG 999 is different from EET 83309 at the 99% confidence limit. Differences in CRE ages indicate each polymict sample was ejected from the parent asteroid in separate events, suggesting each could represent a slightly different mix of materials. Thus, it is not surprising that Nilpena is distinct from other polymict ureilites and that DaG 999 differs from EET 83309. However, the similarity of olivine populations in most polymict ureilites suggests that the regolith is fairly well mixed, and the suite of clasts in each individual polymict ureilite is representative of the material on the parent asteroid within reach of impact gardening.

Polymict ureilites are clastic breccias. A study of their constituent minerals is therefore analogous to provenance studies of terrestrial clastic sedimentary rocks such as sandstones and conglomerates. In such studies, lithic clasts or grains within sedimentary rocks represent material exposed within the hinterland from which the sediment was derived. Certain minerals found in terrestrial sandstones are considered to be diagnostic of derivation from certain rock-types. In an analogous manner, certain common compositions of clasts, such as the ferroan olivines and "Hughes cluster" olivines and augites, can be used as "indicator minerals". DaG 999, DaG 1000, Nilpena and EET 83309 all contain olivine and augite clasts that are identical to olivines and augites from Hughes 009 and lithologies in FRO 93008, FRO 90054 and FRO 90228 (Figs. 2 and 5). The presence of a widespread common composition such as the "Hughes cluster" is unlikely to have occurred if each ureilite represents a different asteroidal body.

From the study of the distribution of different mineral compositions in the polymict ureilites (Fig. 2), it is clear that the exotic ferroan olivines are also quite common. They occur as lithic clasts in the DaG pairing group, EET 83309 and EET 87720 (this work; Ikeda et al., 2000, 2003; Cohen et al., 2004), and as mineral grains in some members of the FRO pairing group (Fioretti and Goodrich, 2001; Smith, 2002). This is unlikely to have been the case if all these samples had been derived from different parent asteroids and also supports the suggestion that the polymict ureilites were all formed on the surface of a single parent asteroid. Given the evidence discussed above that ureilites are derived from a single parent asteroid, it appears that either the asteroid migrated into a region of the nebula that contained R-chondrite-like bodies that were significantly more oxidized, or more likely several oxidized bodies migrated into the region occupied by the ureilite parent body.

Polymict ureilites have been formed near the surface of the ureilite parent asteroid, and those that contain implanted solar wind gases have been formed on the surface, so the range of mineral compositions represents the variety of composition of the rocks present within the outer reaches of the asteroidal surface. A single ureilitic lithic clast in North Haig had an area of 0.7 × 0.6 cm and one from

DaG 1023 was 2 cm long. Therefore, some ureilitic clasts in polymict ureilites must commonly be 1–2 cm in diameter. If most of the FRO ureilites are indeed part of a polymict breccia, as suggested by Welten et al. (2006), then typical clast sizes may be on the order of several cm in diameter for the FRO meteorite group. A significant observation is that polymict ureilites contain both shocked and unshocked ureilitic clasts, and also show a very wide range of compositions of ureilite minerals. This indicates that the surface of the parent asteroid comprises rocks of many different compositions and with widely varying levels of shock. This observation suggests that the original ureilite asteroid experienced asteroid-wide disruption after its initial stages of accretion and melting. Indeed, as discussed below, it is possible that the entire suite of ureilite meteorites, brecciated and unbrecciated, is derived from a coarsely brecciated polymict parent asteroid.

5.5. Models of evolution of the ureilite parent asteroid

Models for the petrogenesis of ureilites are informed by several key observations: (i) ureilites are heterogeneous in oxygen isotopic composition and mg#, and these are correlated (Fig. 7), (ii) ureilites are devoid of plagioclase and have extreme depletions in incompatible elements, (iii) carbon, principally in the form of graphite, is a nearly ubiquitous minor component, (iv) the siderophile element concentrations in ureilites are relatively high, encroaching on the ranges observed for chondrites for some elements, (v) olivine grains have uniform, FeO-bearing cores with FeO-free rims containing Fe metal, and (vi) basaltic material related to ureilites is exceedingly rare, being confined to small fine-grained clasts of low abundance in polymict ureilites. These key observations are embodied in models developed to explain the petrogenesis of ureilites. These models have some commonalities, and contain some controversies.

Ureilites are basalt-depleted, as indicated by the lack of plagioclase and extreme depletions in incompatible elements, and thus the parent asteroid underwent igneous processing. Early models had ureilites formed as cumulates from a magma (e.g., Berkley et al., 1980). However, the discovery of oxygen isotopic heterogeneity among ureilites (Clayton and Mayeda, 1988) made this scenario unpalatable. The current consensus is that ureilites are melt-residues of a heterogeneous parent asteroid (see discussion in Goodrich et al., 2007).

Some argue that reduction by C during melting (smelting) is responsible for the range in silicate mg# of ureilites (Singletary and Grove, 2003, 2006; Goodrich et al., 2004). In this view, the mg# of ureilite olivines is related to the depth at which smelting occurred because the smelting reaction is sensitive to the pressure confining the CO/CO_2 gas produced by the reaction (Singletary and Grove, 2003). The correlation between mg# and oxygen isotopic composition is then explained as indicating that the oxygen isotopic composition was related to depth on the original ureilite parent asteroid (Singletary and Grove, 2003). However, others argue that smelting did not occur at the time of basalt generation (Mittlefehldt et al., 2005; Warren and

Huber, 2006). These authors have shown that there is a negative correlation between bulk rock Fe content and olivine core mg# for unbrecciated ureilites. The smelting model requires the Fe metal be produced during the smelting process. The simplest way to generate the negative bulk rock Fe-olivine mg# correlation would be to systematically drain out the metal produced during smelting. However, as noted by Mittlefehldt et al. (2005) and Warren and Huber (2006), the contents of other siderophile elements do not show a systematic negative correlation with olivine mg#, contrary to a prediction that the smelting model would make. These latter authors consider that the range in silicate mg# was largely inherited from the protolith, with only minor changes caused by normal igneous melting. At present, there is no consensus regarding whether smelting was an important process during ureilite formation.

The dearth of basaltic material in the ureilite suite is commonly explained as the result of explosive volcanism having blasted volcanic ash into space with high enough velocity to escape the asteroid (Warren and Kallemeyn, 1992; Scott et al., 1993; Goodrich et al., 2004). Because ureilites ubiquitously contain graphite, the proponents of this model assume some of the graphite will be entrained by the rising magma. As the magma approaches the surface of the asteroid, the lower pressure promotes reduction of FeO in the magma by graphite, producing CO/CO_2. At low enough pressure, CO/CO_2 exsolve into a gas phase fragmenting the melt and acting as the propellant fueling explosive volcanism (Warren and Kallemeyn, 1992; Scott et al., 1993; Goodrich et al., 2004). While this is a physically plausible model for volcanism on the ureilite parent asteroid, there is no direct evidence supporting this process. It is only the presence of graphite in ureilites and the lack of basalts that supports it.

Researchers agree that the reduced rims on olivine grains were caused by sudden pressure release at high temperature. Singletary and Grove (2003) calculate that the cores of olivine and pigeonite were in equilibrium at temperatures in the range 1150–1300 °C before the reduced rims were formed. The more ferran ureilites must have been under modest pressure at these temperatures to prevent FeO reduction of the olivine cores (Singletary and Grove, 2003). Modeling of diffusion profiles for the reduced rims on olivine grains for three ureilites yield cooling rate estimates of 2–6° per hour (Miyamoto et al., 1985), implying a sudden decrease in pressure allowing for reduction and rapid cooling. This event is typically associated with

impact unroofing of the original ureilite asteroid mantle (e.g., see Mittlefehldt et al., 1998). The universality of this characteristic reduced-rim texture among unbrecciated ureilites implies that the event affected much, if not all, of the original ureilite asteroid. Hence, a simple cratering event seems insufficient. This has led to a model whereby the original "proto-ureilite" asteroid suffered a catastrophic disruption by impact that halted igneous processing, generated the reduced rims through the sudden pressure drop, and "scrambled" the original interior during reassembly of the fragments. This mixing caused material with a range of silicate mg#s and shock levels to lie within impact gardening range on the ureilite parent asteroid (e.g., see Goodrich et al., 2004).

Catastrophic impact disruption-reassembly models have been invoked to explain the petrologic-chemical characteristics of other meteorite groups. Scott et al. (2001) have interpreted the mesosiderite metal-silicate polymict breccias to have arisen on a differentiated asteroid by such a mechanism. In their model, a 200–400 km diameter differentiated target asteroid was impacted by a 50–150 km diameter impactor asteroid, disrupting the target asteroid and mixing core metal and crustal silicates to form mesosiderites. Benedix et al. (2000) called upon a disruption-reassembly model to mix materials from various depths and generate the winonaite-IAB iron suite of meteorites. In both of these cases, scrambling of material from different depths on the target asteroid is hypothesized to have occurred as a result of this process.

Asphaug et al. (2006) have modeled the physics of planetary embryo impacts. They show that under some conditions, oblique impacts can result in the impactor emerging from the encounter with its outer layers removed, but the interior largely intact. This is a potential alternative explanation for the paucity of basaltic material associated with ureilites; the basaltic surface and some of the mantle of the original asteroid was stripped-off during an encounter with a planetary embryo. However, this would not necessarily explain the range in mg# of ureilite material in the polymict breccias unless it was all within range of subsequent impact gardening of the post-impact daughter asteroid that became the ureilite parent asteroid. It may be possible within the framework of an Asphaug-like model if the outer layers of the original ureilite parent asteroid were more deeply removed on some parts compared to others. The physical modeling is not detailed enough at this point to address

Table 4
Results of non-parametric Mann–Whitney two-tailed test on olivine mg#s for individual polymict ureilites

	DaG 999	DaG 1000	EET 83309	EET 87720	Nilpena	North Haig
DaG999 (71)		Same	Different	Same	Different	Same
DaG 1000 (45)			Same	Same	Different	Same
EET 83309 (61)				Same	Different	Same
EET 87720 (63)					Different	Same
Nilpena (60)						Different
North Haig (41)						

"Same" indicates the two populations are statistically the same at the 99% confidence level. Numbers in parentheses are the number of olivine grains in the data set.

this possibility. In addition, impactor fragmentation does occur in some cases (Asphaug et al., 2006). Re-accretion of some of the fragments would result in a "rubble pile" ureilite parent asteroid as envisioned by Goodrich et al. (2004) as the asteroid upon which the polymict ureilites were formed by impact gardening.

We suggest that an encounter between a large proto-ureilite asteroid and a possibly Moon-sized target could explain three of the characteristics of ureilites: (i) efficient removal of a basaltic crust, (ii) sudden pressure drop causing reduction of olivine grain margins, and (iii) exposure of mantle material having a range in mg# and oxygen isotope ratios for inclusion in the ureilite suite and polymict breccias. This eliminates the need for explosive volcanism to expel basaltic material off the original ureilite asteroid, and thus simplifies the model for ureilite origins. Asphaug et al. (2006) presented only a subset of models in which the target was Mars-sized and the impactors were either half that size, or a tenth that size (roughly Moon-sized). Modeling of an encounter between a Ceres-sized impactor and Moon-sized target would allow for testing of our suggested scenario.

6. CONCLUSIONS

A petrological study of ureilitic silicate mineral clasts in six polymict ureilites has revealed that each polymict ureilite contains a wide range of olivine and pyroxene compositions, exactly covering the Fe–Mg–Mn compositional range seen among unbrecciated ureilites. The olivine mg# distribution in the studied polymict ureilites is statistically indistinguishable from that of the unbrecciated ureilite suite, indicating that they sample the same olivine population. High precision in situ SIMS oxygen isotope data for clasts from two polymict samples also cover the range shown by bulk analyses of unbrecciated ureilites. "Indicator minerals", such as olivines and augites derived from material similar to Hughes 009, are present in several different polymict ureilites. Together, these observations are interpreted to indicate that all ureilites were derived from a single parent asteroid.

Exotic ferroan olivines derived from R-chondrites and another oxidized asteroid are also present on the surface of the ureilite asteroid, as also confirmed by the SIMS oxygen isotope analyses. Mineral compositions and O isotope data show that enstatite chondrite or achondrite materials, and material from an unknown meteorite type are present, and petrologic evidence shows that other exogenous grains are present. Combining our and literature data, we estimate that at least six distinct major impactor types are represented in the polymict breccias. The presence of rarer exogenous grains suggests that there were other, less well-represented impactors.

Ureilites fall into two main groups, according to the mg# and Mn contents of their olivines. Those with mg# < 85 show a coherent negative trend of FeO vs. MnO in olivines, whereas those with mg#s > 85 are much more scattered. The more magnesian group includes the "Hughes cluster" materials, which contain melt inclusions. Poikilitic textures are also common within this group.

These data are interpreted to indicate that magnesium-rich partial melts were still present in the proto-ureilite asteroid when it was disrupted by impact, and these melts became impregnated into the residual mantle to form "Hughes cluster" rocks.

After such a disruption, at least one daughter ureilite asteroid accreted at a much lower temperature, forming a rubble-pile body. The occurrence of mafic silicate minerals showing a wide range of mg#s in all of the polymict ureilites investigated in this study indicates that all of this material was within impact gardening depth of the surface of the daughter asteroid during regolith formation. Regolith formation began and impacts from a wide range of other bodies occurred, including showers of material from both more oxidized and more reduced asteroids having a wide range in oxygen isotopic compositions.

APPENDIX A. SUPPLEMENTARY DATA

Supplementary data associated with this article can be found, in the online version, at doi:10.1016/ j.gca.2008.06.028.

REFERENCES

Aléon J., Krot A. N. and McKeegan K. D. (2002) Calcium–aluminum-rich inclusions and amoeboid olivine aggregates from the CR carbonaceous chondrites. *Meteoritics Planet. Sci.* **37**, 1729–1755.

Asphaug E., Agnor C. B. and Williams Q. (2006) Hit-and-run planetary collisions. *Nature* **439**, 155–160.

Benedix G. K., McCoy T. J., Keil K. and Love S. G. (2000) A petrologic study of the IAB iron meteorites: constraints on the formation of the IAB-winonaite parent body. *Meteoritics Planet. Sci.* **35**, 1127–1141.

Benedix G. K., Lauretta D. S. and McCoy T. J. (2005) Thermodynamic constraints on the formation conditions of winonaites and silicate-bearing IAB irons. *Geochim. Cosmochim. Acta* **69**, 5123–5131.

Berkley J. L. (1986) Four Antarctic ureilites: petrology and observations on ureilite petrogenesis. *Meteoritics* **21**, 169–189.

Berkley J. L., Taylor G. J., Keil K., Harlow G. E. and Prinz M. (1980) The nature and origin of ureilites. *Geochim. Cosmochim. Acta* **44**, 1579–1597.

Bischoff A., Geiger T., Palme H., Spettel B., Schultz L., Scherer P., Loeken T., Bland P., Clayton R. N., Mayeda T. K., Herpers U., Meltzow B., Michel R. and Dittrich-Hannen B. (1994) Acfer 217—a new member of the Rumuruti chondrite group (R). *Meteoritics* **29**, 264–274.

Brearley A. J. and Jones R. H. (1998) Chondritic meteorites. In *Planetary Materials*, (ed. J. J. Papike), Reviews in Mineral, vol. 36. Mineralogical Society of America, Washington, DC, pp. 3-1–3-398.

Brearley A. J. and Prinz M. (1992) CI chondrite-like clasts in the Nilpena polymict ureilite: implications for aqueous alteration processes in CI chondrites. *Geochim. Cosmochim. Acta* **56**, 1373–1386.

Clayton R. N. and Mayeda T. K. (1988) Formation of ureilites by nebular processes. *Geochim. Cosmochim. Acta* **52**, 1313–1318.

Clayton R. N. and Mayeda T. K. (1996) Oxygen isotope studies of achondrites. *Geochim. Cosmochim. Acta* **60**, 1999–2017.

Clayton R. N., Mayeda T. K. and Rubin A. E. (1984) Oxygen isotopic compositions of enstatite chondrites and aubrites. *Proc. Part 1, J. Geophys. Res.* **89**(Suppl.), C245–C249.

Cohen B., Goodrich C. A. and Keil K. (2004) Feldspathic clast populations in polymict ureilites: stalking the missing basalts from the ureilite parent body. *Geochim. Cosmochim. Acta* **68**, 4249–4266.

Downes H. (1997) Shallow continental lithospheric mantle heterogeneity—petrological constraints. In *Upper Mantle Heterogeneities from Active and Passive Seismology* (ed. K. Fuchs). Kluwer Academic Publications, The Netherlands, pp. 295–308.

Fioretti A. M. and Goodrich C. A. (2000) Primary melt inclusions in olivine, augite and orthopyroxene in ureilite FRO 90054. *Lunar Planet. Sci.* **31**, #1202.

Fioretti A. M. and Goodrich C. A. (2001) A contact between an olivine-pigeonite lithology and an olivine-augite-orthopyroxene lithology in ureilite FRO 93008: dashed hopes? *Meteoritics Planet. Sci.* **36**, A58.

Franchi I. A., Sexton A. S., Wright I. P. and Pillinger C. T. (1997) Resolved sub-groups within the ureilite population. *Meteoritics Planet. Sci.* **32**, A44.

Goodrich C. A. (1986) Y74130: a ureilite with cumulus augite. *Meteoritics* **21**, 373–374.

Goodrich C. A. (1992) Ureilites—a critical review. *Meteoritics* **27**, 327–352.

Goodrich C. A. (2001) Magmatic inclusions in Frontier Mountains 90054 and Elephant Moraine 96328: complex petrogenesis of the olivine-(augite)-orthopyroxene ureilites. *Lunar Planet. Sci.* **32**, #1300.

Goodrich C. A., Jones J. H. and Berkley J. L. (1987) Origin and evolution of ureilite parent magmas: multi-stage igneous activity on a large parent body. *Geochim. Cosmochim. Acta* **51**, 2255–2273.

Goodrich C. A., Fioretti A. M., Tribaudino M. and Molin G. (2001) Primary trapped melt inclusions in olivine in the olivine-augite-orthopyroxene ureilite Hughes 009. *Geochim. Cosmochim. Acta* **65**, 621–652.

Goodrich C. A., Hutcheon I. D. and Keil K. (2002) ^{53}Mn–^{53}Cr age of a highly evolved, igneous lithology in polymict ureilite DaG 165. *Meteoritics Planet. Sci.* **37**, A54.

Goodrich C. A., Scott E. R. D. and Fioretti A. M. (2004) Ureilitic breccias: clues to the petrological structure and impact disruption of the ureilite parent asteroid. *Chemie der Erde* **64**, 283–327.

Goodrich C. A., Van Orman J. A. and Wilson L. (2007) Fractional melting and smelting on the ureilite parent body. *Geochim. Cosmochim. Acta* **71**, 2876–2895.

Guan Y. and Crozaz G. (2000) Light rare earth element enrichments in ureilites: a detailed ion microprobe study. *Meteoritics Planet. Sci.* **35**, 131–144.

Guan Y. and Crozaz G. (2001) Microdistributions and petrogenetic implications of rare earth elements in polymict ureilites. *Meteoritics Planet. Sci.* **36**, 1039–1956.

Ikeda Y. and Prinz M. (2001) Magmatic inclusions and felsic clasts in the Dar al Gani 319 polymict ureilite. *Meteoritics Planet. Sci.* **36**, 481–499.

Ikeda Y., Prinz M. and Nehru C. E. (2000) Lithic and mineral clasts in the Dar al Gani (DAG) 319 polymict ureilite. *Antarctic Meteorite Res.* **13**, 177–221.

Ikeda Y., Kita N. T., Morishita Y. and Weisberg M. K. (2003) Primitive clasts in the Dar al Gani 319 polymict ureilite: precursors of the ureilites. *Antarctic Meteorite Res.* **16**, 105–127.

Jaques A. L. and Fitzgerald M. J. (1982) The Nilpena ureilite, an unusual polymict breccia: implications for origin. *Geochim. Cosmochim. Acta* **46**, 893–900.

Jones R. H., Leshin L. A., Guan Y. B., Sharp Z. D., Durakiewicz T. and Schilk A. J. (2004) Oxygen isotope heterogeneity in chondrules from the Mokoia CV3 carbonaceous chondrite. *Geochim. Cosmochim. Acta* **68**, 3423–3438.

Karner J., Papike J. J. and Shearer C. K. (2003) Olivine from planetary basalts: chemical signatures that indicate planetary parentage and those that record igneous setting and process. *Am. Min.* **88**, 806–816.

Kita N. T., Ikeda Y., Morishita Y. and Togashi S. (2003) Timing of basaltic volcanism in ureilite parent body inferred from the ^{26}Al ages of plagioclase-bearing clasts in DaG-319 polymict ureilite. *Lunar Planet Sci.* **34**, #1557.

Kita N. T., Ikeda Y., Togashi S., Liu Y., Morishita Y. and Weisberg M. K. (2004) Origin of ureilites inferred from a SIMS oxygen isotopic and trace element study of clasts in the Dar al Gani 319 polymict ureilite. *Geochim. Cosmochim. Acta* **68**, 4213–4235.

Kita N. T., Ushikubo T., Fu B., Spicuzza M. J. and Valley J. W. (2007) Analytical developments on oxygen three isotope analyses using a new generation ion microprobe IMS-1280. *Lunar Planet. Sci.* **38**, #1981.

Krot A. N., Libourel G. and Cahussidon M. (2006) Oxygen isotope compositions of chondrules in CR chondrites. *Geochim. Cosmochim. Acta* **70**, 767–779.

Lee D. C., Halliday A. N., Singletary S. J. and Grove T. L. (2005) ^{182}Hf–^{182}W chronometry and an early differentiation in the parent body of ureilites. *Lunar Planet. Sci.* **36**, #1638.

Mittlefehldt D. W. (1986) Fe–Mg–Mn relations of ureilite olivines and pyroxene and the genesis of ureilites. *Geochim. Cosmochim. Acta* **50**, 107–110.

Mittlefehldt D. W., McCoy T. J., Goodrich C. A. and Kracher A. (1998) Non-chondritic meteorites from asteroidal bodies. In *Planetary Materials*, (ed. J. J. Papike), Reviews in Mineral, vol. 36. Mineralogical Society of America, Washington, DC, pp. 4-1–4-195.

Mittlefehldt D. W., Bogard D. D., Berkley J. L. and Garrison D. H. (2003) Brachinites: igneous rocks from a differentiated asteroid. *Meteoritics Planet. Sci.* **38**, 1601–1625.

Mittlefehldt D. W., Hudon P. and Galindo, Jr., C. (2005) Petrology, geochemistry and genesis of ureilites. *Lunar Planet. Sci.* **36**, #1040.

Miyamoto M., Takeda H. and Toyoda H. (1985) Cooling history of some Antarctic ureilites. *Proc. 16th Lunar Planet. Sci. Conf., Part 1, J. Geophys. Res.* **90**(Suppl.), D116–D122.

Ogata H., Mori H. and Takeda H. (1991) Mineralogy of interstitial rim materials of the Y74123 and Y790981 ureilites and their origin. *Meteoritics* **26**, 195–201.

Prinz M., Delaney J. S., Nehru C. E. and Weisberg M. K. (1983) Enclaves in the Nilpena polymict ureilite. *Meteoritics* **18**, 376.

Prinz M., Weisberg M. K., Nehru C. E. and Delaney J. S. (1986) North Haig and Nilpena: paired polymict ureilites with Angra

dos Reis-related and other clasts. *Lunar Planet. Sci.* **17**, 681–682.

Prinz M., Weisberg M. K., Nehru C. E. and Delaney J. S. (1987) EET 83309, a polymict ureilite: recognition of a new group. *Lunar Planet. Sci.* **18**, 802–803.

Rai V. K., Murthy A. V. S. and Ott U. (2003) Noble gases in ureilites: cosmogenic, radiogenic and trapped components. *Geochim. Cosmochim. Acta* **67**, 4435–4456.

Russell S. S., Zipfel J., Folco L., Jones R., Grady M. M., McCoy T. and Grossman J. N. (2003) The Meteoritical Bulletin, No. 87. *Meteoritics Planet. Sci.* **38**, A189–A248.

Shulze H., Bischoff A., Palme H., Spettel B., Dreibus G. and Otto J. (1994) Mineralogy and chemistry of Rumuruti: the first meteorite fall of the new R chondrite group. *Meteoritics* **29**, 275–286.

Scott E. R. D., Taylor G. J. and Keil K. (1993) Origin of ureilite meteorites and implications for planetary accretion. *Geophys. Res. Lett.* **20**, 415–418.

Scott E. R. D., Haack H. and Love S. G. (2001) Formation of mesosiderites by fragmentation and reaccretion of a large differentiated asteroid. *Meteoritics Planet. Sci.* **36**, 869–881.

Singletary S. J. and Grove T. L. (2003) Early petrologic processes on the ureilite parent body. *Meteoritics Planet. Sci.* **38**, 95–108.

Singletary S. and Grove T. L. (2006) Experimental constraints on ureilite petrogenesis. *Geochim. Cosmochim. Acta* **70**, 1291–1308.

Smith C. L. (2002) An integrated, mineralogical, petrologic and isotopic study of ureilites. Ph.D. dissertation, Open University.

Takeda H. (1987) Mineralogy of Antarctic ureilites and a working hypothesis for their origin and evolution. *Earth Planet. Sci. Lett.* **81**, 358–370.

Takeda H., Mori H. and Ogata H. (1989) Mineralogy of augite-bearing ureilites and the origin of their chemical trends. *Meteoritics* **24**, 73–81.

Torigoye-Kita N., Tatsumoto M., Meeker G. P. and Yanai K. (1995) The 4.56 Ga U–Pb age of the MET 78008 ureilite. *Geochim. Cosmochim. Acta* **59**, 2319–2329.

Treiman A. H. and Berkley J. L. (1994) Igneous petrology of the new ureilites Nova 001 and Nullabor 010. *Meteoritics* **29**, 843–848.

Wahl W. (1952) Brecciated stony meteorites and meteorites containing foreign fragments. *Geochim. Cosmochim. Acta* **2**, 91–117.

Walker D. and Grove T. L. (1993) Ureilite smelting. *Meteoritics* **28**, 629–636.

Warren P. H. and Huber H. (2006) Ureilite petrogenesis: a limited role for smelting during anatexis and catastrophic disruption. *Meteoritics Planet. Sci.* **41**, 835–849.

Warren P. H., Ulff-Moller F., Huber H. and Kallemeyn G. W. (2006) Siderophile geochemistry of ureilites: a record of early stages of planetesimal core formation. *Geochim. Cosmochim. Acta* **70**, 2104–2126.

Warren P. and Kallemeyn G. W. (1989) Geochemistry of polymict ureilite EET 83309, and a partially-disruptive impact model for ureilite origin. *Meteoritics* **24**, 233–246.

Warren P. and Kallemeyn G. W. (1992) Explosive volcanism and the graphite–oxygen fugacity buffer on the parent asteroid(s) of the ureilite meteorites. *Icarus* **100**, 110–126.

Weisberg M. K., Prinz M., Kojima H., Yanai K., Clayton R. N. and Mayeda T. K. (1991) The Carlisle Lakes-type chondrites: a new grouplet with high $\Delta^{17}O$ and evidence for nebular oxidation. *Geochim. Cosmochim. Acta* **55**, 2657–2669.

Welten K. C., Nishiizumi K., Caffee M. W. and Hillegonds D. J. (2006) Cosmogenic radionuclides in ureilites from Frontier Mountains, Antarctica: evidence for a polymict breccia. *Lunar Planet. Sci.* **37**, #2391.

Young E. D. and Russell S. S. (1998) Oxygen reservoirs in the early solar nebula inferred from an Allende CAI. *Science* **282**, 452–455.

Zolensky M. E., Weisberg M. K., Buchanan P. C. and Mittlefehldt D. W. (1996) Mineralogy of carbonaceous chondrite clasts in HED achondrites and the moon. *Meteoritics Planet. Sci.* **31**, 518–537.

Associate editor: Hiroko Nagahara